DANMARKS OG GRØNLANDS GEOLOGISKE UNDERSØGELSE **RAPPORT 2023/43**

FINGERSEG, Fingerprinting Caledonian tectono-thermal events in South-East Greenland using low temperature U-Th/Pb and Ar/Ar Geochronology

Pierpaolo Guarnieri, Tonny B. Thomsen,
Benjamin Heredia & Michael Storey

GEOLOGICAL SURVEY OF DENMARK AND GREENLAND
DANISH MINISTRY OF CLIMATE, ENERGY AND UTILITIES

GEUS

DANMARKS OG GRØNLANDS GEOLOGISKE UNDERSØGELSE **RAPPORT 2023/43**

FINGERSEG, Fingerprinting Caledonian tectono-thermal events in South-East Greenland using low temperature U-Th/Pb and Ar/Ar Geochronology

[1]Pierpaolo Guarnieri, [1]Tonny B. Thomsen, [1]Benjamin Heredia & [2]Michael Storey

[1]Geological Survey of Denmark and Greenland (GEUS), Department of Mapping and Mineral Resources, Øster Voldgade 10, 1350 Copenhagen, Denmark

[2]University of Copenhagen, Natural History Museum of Denmark, Quadlab, Gothersgade 130, 1123 Copenhagen, Denmark

GEOLOGICAL SURVEY OF DENMARK AND GREENLAND
DANISH MINISTRY OF CLIMATE, ENERGY AND UTILITIES

GEUS

Index

1. Introduction

The project FINGERSEG is a geochronology-based study funded by Geocenterbevilling 6-2017. Aim of the project is to find evidence of Palaeozoic (i.e. Caledonian) tectono-thermal overprint on rock-samples collected in South-East Greenland. The collaboration between GEUS and the Geological Museum gave the possibility to analyse rock samples for U-Th/Pb and Ar/Ar age dating in order to investigate low temperature thermal events in South-East Greenland.

The reason to investigate for Caledonian-age events in South-East Greenland was due to a new analysis (Thomsen and Guarnieri pers. comm.) of detrital rutile obtained from a drop-stone of red beds collected in the Ammassalik area (Lat. 66ºN) in South-East Greenland (Dawes, 1986). The rock analysed for detrital zircon showed Archaean to Palaeoproterozoic ages but the U-Th/Pb age of detrital rutile resulted in robust Silurian ages (ca. 430 Ma) in addition to a single Palaeoproterozoic rutile age at 1800 Ma. This surprising result came from an erratic rock, probably transported from the north-west, suggesting that such a type of rocks should be present nearby under the ice cap.

2. Background

Ordovician-Silurian rocks were discovered to the north in the Kangerlussuaq area (Lat. 68ºN) by Brooks et al. (1981) belonging to the Batbjerg intrusion that is surrounded by Lower Palaeozoic marbles and metasandstones (Fig. 1).

Evidence for Caledonian-age cooling events are shown by apatite fission tracks analysed on samples collected in the Skjoldungen and Ammassalik areas (Fig. 1) during the SEGMENT Project in South East Greenland (Guarnieri 2014; Guarnieri et al. 2014; Green et al. 2014; Kolb et al. 2016). The data show clear Ordovician-Silurian cooling ages that can be interpreted as post-Caledonian exhumation.

Moreover, greenschist facies metasandstones were encountered during the ODP Leg 152 Hole 917A located offshore Skjoldungen (Lat. 64ºN) in South East Greenland (Fig. 1). The drill went through ca. 779 m of Tertiary basalts and then 10 cm of quartz-sandstones. After the quartz-sandstone the drill recovered 53.7 m of steeply dipping and metamorphosed (greenschist facies) sandstones and siltstones (Vallier et al. 1998). The authors interpreted the metasandstones as Upper Cretaceous in age and correlate it with the Kangerlussuaq Basin to the north.

The presence of un-metamorphosed quartz-sandstones between the metasandstones and the Tertiary basalts above, suggests that the greenschist facies event is not related to Tertiary activity but should be older (Caledonian?). In 2015 four samples from Leg 152/917A were requested to the ODP repository and analysed at GEUS for detrital zircon and rutile to estimate the maximum age of the rocks. Unfortunately no heavy mineral were found, thus the age is still unknown, however anticipated to be of Lower Palaeozoic age.

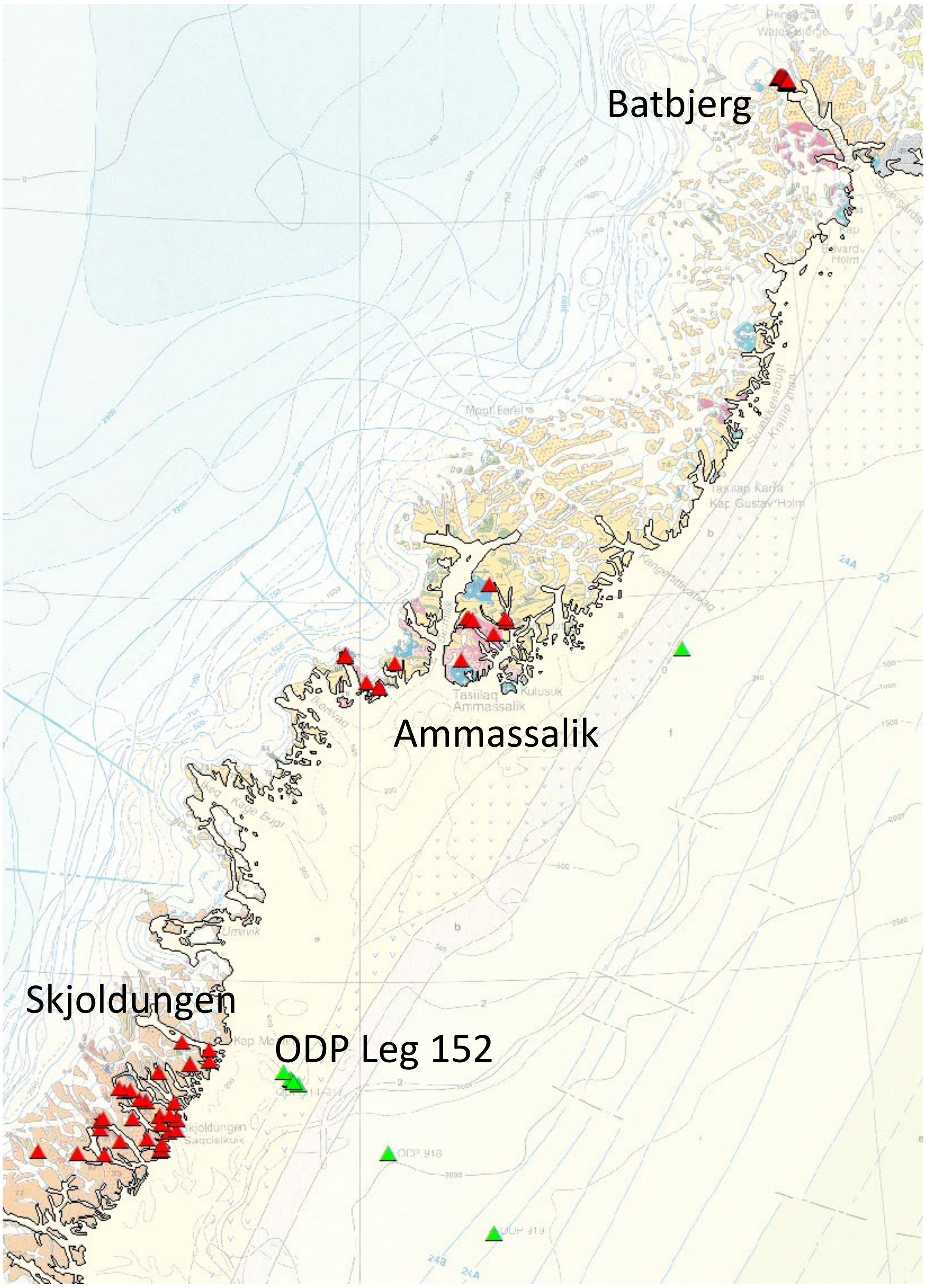

Fig. 1. Samples distribution from Skjoldungen-Ammassalik (SEGMENT project) and Batbjerg (red) and from ODP Leg 152 (green).

3. Analytical work

The following rock samples are available and considered to be analysed in FINGERSEG project:

- 4-6 Core samples from ODP Leg 152/917: Ar/Ar age dating of biotite/muscovite by Michael Storey at the Geological Museum’s Argon Geochronology laboratory.
- 40 Basement rock samples from South-East Greenland: U-Th/Pb age dating of titanite/monazite/rutile/apatite (LA-ICPMS facility at GEUS);
- 10 Basement rock and metasediment samples from the Batbjerg area in Kangerlussuaq, East Greenland (collected by K. Brooks, available and stored at the Geological Museum): U-Th/Pb age dating of titanite/monazite/rutile/apatite (LA-ICPMS facility at GEUS).
- 10 Basement rock samples from Mont Forel-Glacier de France area in South-East Greenland (collected by the British Army in 2016 and stored at GEUS; see Fig. 1): U-Th/Pb age dating of titanite/monazite/rutile/apatite (LA-ICPMS facility at GEUS).

4. Methods

4.1 $^{40}Ar/^{39}Ar$ dating

For 40Ar/39Ar age determination whole-rock mini-cores and biotite crystal separates were loaded into pits in aluminum irradiation disks. Each unknown was surrounded the neutron flux monitor Fish Canyon sanidine (FCs) with an assigned age of 28.201 (Kuiper et al., 2008). The irradiation disks were then wrapped in aluminum foil and encapsulated in a heat-sealed quartz glass tube. The samples were irradiated in the cadmium-lined in-core (CLICIT) facility at the Oregon State University TRIGA reactor for 9 hours. Argon isotopic analyses of the gas released by laser step-heating of the whole-rock mini-cores and biotite separates (Supplementary data) were made on a fully automated, high-resolution Nu Instruments Noblesse multi-collector noble-gas mass spectrometer (Nu Instruments) at the Natural History Museum of Denmark, using previously documented instrumentation and procedures (Storey et al., 2007, Rivera et al., 2011). The data are reported relative to the astronomically calibrated 40Ar/39Ar age of 28.201 Ma for the Fish Canyon sanidine monitor mineral (Kuiper et al., 2008).

4.2 U-Th/Pb dating

U/Pb geochronology was carried out by laser ablation inductively coupled plasma mass spectrometry (LA-ICPMS) at GEUS. The U/Pb dating were performed in-situ on the same polished rock chip of sample 103R as for the Ar/Ar dating. Based on the AQM screening analysis, apatite mineral grains of preferably > 20 um in size were selected for the LA-ICPMS dating. The location of each apatite mineral grain as identified by the AQM and BSE images were transferred to the LA-ICPMS instrument by using a linear transformation matrix from the two coordinated frames, using six reference points, and thereby matching the position between the three (AQM + BSE images and LA-ICPMS instrument). A NWR 213 frequency-quintupled solid state Nd:YAG laser system from Elemental Scientific Lasers (ESL) mounted with a standard TV2 ablation cell was coupled to an ELEMENT 2 double-focusing single-collector magnetic sector-field ICPMS from Thermo-Fisher Scientific. The mass spectrometer is equipped with a new jet interface pump system, a detector amplifier, and employed Ni jet-type sampler and standard H-type skimmer cones. Operating conditions and data acquisition parameters are listed in Appendix 1. Prior to loading, the chip section and standards were carefully cleaned with ethanol to remove possible surface contamination. To ensure stable laser output energy, the laser was heated prior to operation, providing a stable laser power and flat ablation craters. The mass spectrometer was run for at least one hour before analysis to stabilize the background signal. The ablated material was swept by the helium carrier gas and mixed with argon gas ca. 0.5 m before entering the mass spectrometer. The ICP-MS was optimized for dry plasma conditions through continuous linear ablation of the GJ-1 zircon standard. The signal-to-noise ratios for the heavy mass range of interest (i.e. 202Hg to 238U), emphasizing on 238U and 206Pb, were maximized, while simultaneously opting for the lowest element-oxide production level by minimizing the UO2/U ratio. To minimize instrumental drift, a standard-sample-standard analysis protocol was followed, bracketing 7-8 samples by 4 standard measurements for each bracket. Standard analyses and results were validated by analyses of the natural apatite standards McClure (Schoene and Bowring 2006) and Durango (Chew et al. 2011), and the Plešovice (Slama et al. 2008) and GJ-1 (Jackson et al. 2004) zircon standards. All standards demonstrated an averaged age accuracy within 3% deviation (2σ) from reference values, and internal uncertainties of < 2-3% (2σ). Data processing was performed off-line using the software Iolite v. 2.5 (Paton et al. 2010, 2011) with the VizualAge data reduction scheme (Petrus & Kamber 2012). Data were corrected for background, session drift and down-hole isotopic fractionation by using GJ-1 as the primary reference material. Data was acquired from single spot analysis using a laser spot size of for the analyses of 25 µm. A laser fluence of ca. 3 J/cm2 and a pulse rate of 5 Hz was applied. Acquisition sequence included 30 s background measurement, then laser ablation on for 40 s, and finally washout for 40 s. Factory-supplied software was used for the acquisition of the transient data, obtained through automated running mode of pre-set analytical locations.

Apatite usually require common Pb correction. However, for apatites with a high proportion of common Pb, assumption that the common Pb ratio is invariant will mean that any error in the isotope ratios assigned to common Pb will result in a consistent bias, rather than a random, of the calculated 206Pb/238U and 207Pb/206Pb radiogenic ratios (Ludwig, 1998). Thus, using a ‘‘SemiTotal–Pb/U isochron’’ approach (Tera and Wasserburg, 1972), the background- and session-drift corrected ratios can be plotted on the Tera-Wasserburg concordia diagram without correction for common Pb. If (and only if) the true 206Pb/238U and 207Pb/206Pb radiogenic isotope ratios represent comparable dates, the non-common Pb corrected data will be dispersed along a line whose lower intercept with the concordia curve defines the age of the episode responsible for this line (Ludwig, 1998). This is the case for the apatite grains herein, and thus the lower intercept age reported here for the apatites is not corrected for common Pb, assuming that this intercept age denotes the U/Pb isotopic age of a specific geological event recorded by the apatite mineral grains. Diagrams and statistical information were produced through the software IsoplotR (Vermeesch 2018).

5. Results

5.1 U-Th/Pb and Ar/Ar age dating of rock samples from ODP Leg 152

This chapter is represented by the paper published on Geological Magazine in 2022.

First evidence for Neoproterozoic rocks offshore South-East Greenland

***Pierpaolo Guarnieri[1], Michael Storey[2], Tonny B. Thomsen[1], Benjamin Dominguez Heredia[1], Sebastian Næsby Malkki[1]**

[1]Geological Survey of Denmark and Greenland (GEUS), Department of Petrology and Economic Geology, Øster Voldgade 10, 1350 Copenhagen

[2]Quadlab Natural History Museum of Denmark, Gothersgade 130, 1123 Copenhagen

*Correspondence (pgua@geus.dk)

ABSTRACT

Meta-sedimentary rocks recovered beneath Paleogene basalts near the base of the ODP Leg 152-917A offshore South-East Greenland were thought to be of Late Cretaceous age. This interpretation, however, has several inconsistencies as it requires a tectono-metamorphic event during the Cretaceous not recognized in the North Atlantic region, and the presence of a wide Mesozoic sedimentary basin that extended from SE-Greenland to the Rockall Plateau, for which there is currently no evidence. Here, we report a Neoproterozoic U/Pb apatite age of 905±21 Ma and a slightly younger $^{40}Ar/^{39}Ar$ isochron whole-rock age of 820±40 Ma for an altered tuff layer that occurs in the upper part of the meta-volcaniclastic sequence recovered from Hole 917A. The $^{40}Ar/^{39}Ar$ step-heating ages on biotite and whole-rock mini-cores from deeper in the Hole 917A yielded Paleoproterozic dates that cluster around 1950 to 1850 Ma, pointing toward a Paleoproterozoic source. The U/Pb apatite date is interpreted as the eruption age of the tuff layer, whereas the slightly younger whole-rock $^{40}Ar/^{39}Ar$ age is consistent with low-temperature greenschist alteration of volcanic glass and secondary mineral growth during sedimentary burial in an extensional regime. The ca. 905 Ma age for the tuff provides the first evidence for Neoproterozoic rocks offshore South-East Greenland and suggests a correlation between this sequence and the Torridon Group in the Hebridean Foreland of the Scottish Caledonides. The calc-alkaline nature of the volcaniclastic rocks and the

age of the tuff layer point toward a source area with arc-magmatism related to the Renlandian event of the Valhalla Orogeny.

1. Introduction

The South-East Greenland offshore area is dominated by the Paleogene volcanic province (Fig. 1), which is associated with the opening of the North Atlantic (Larsen & Saunders 1998). This province was the target for the ODP Leg 152 drilling and sampling of volcanic rocks for geochronology and geochemistry to improve our knowledge of the East Greenland Large Igneous Province (Larsen & Saunders 1998; Tegner et al. 1998; Storey et al. 2007). At site 917 of the ODP Leg 152 ~53.7 m of steeply dipping metasedimentary rocks was drilled beneath >800 m of Paleocene basalts (Vallier et al., 1998). Ten centimeters of quartz sandstone, probably of fluvial origin, was recovered between the basalt and metamorphosed sedimentary rocks (Vallier et al., 1998).

The onshore area along SE Greenland is characterized by the Archean North Atlantic Craton orthogneisses and supracrustal rocks together with Paleoproterozoic Nagssugtoqidian Orogen-related magmatic rocks and gneisses. In the Ammassalik area an early Mesoproterozoic batholith are documented (Kolb, 2014). North of Ammassalik, the nearest known Mesozoic sediments are located at Kap Gustav Holm and further north, where Cretaceous–Paleocene sedimentary rocks belong to the Kangerlussuaq Basin (Larsen et al., 1999). The basin consists of a ca. 1 km thick Cretaceous to Paleocene sedimentary succession (Larsen et al. 1999) onlapping Archean basement gneisses. The sedimentary rocks belong to the Kangerlussuaq Group and the volcano-sedimentary package to the Blosseville group (Soper et al. 1976; Nielsen et al. 1981). The basin and the inland area were covered by a thick pile of plateau basalts in the Early Eocene and overprinted by Paleogene magmatism related to the break-up of the NE-Atlantic Ocean.

The fluvial quartz-sandstone drilled in Core 917A, which unconformably overlies the metasedimentary package, is texturally immature and probably sourced from a deeply weathered basement terrane. Contacts between mineral grains are sharp and un-sutured, indicating that minimal recrystallization occurred. This is also supported by unaltered micas and plagioclase feldspar grains with a high calcium content, of which some show well-developed twinning (Vallier et al. 1998). On the contrary, the metamorphic grade of rocks underneath the angular unconformity reached the lower end of the greenschist facies window, and which is considerably higher than the metamorphism of the basalts (Demant et al., 1998), This suggests an earlier and stronger metamorphic overprint that, in absence of a cleavage indicating a major folding event, was interpreted by Vallier et al. (1998) as tilting caused by rifting processes. They showed that the metasedimentary rocks were significantly deformed and overprinted compared to the quartz-sandstone, and concluded that they were metamorphosed, tilted, uplifted and eroded during the Late Cretaceous-Paleocene before the quartz sandstone was deposited and the basalt flows emplaced. The age of the metasedimentary package was not resolved, and these rocks were assumed to be analogues to the Cretaceous-Paleocene sediments of the Kangerlussuaq Basin (Fig. 1). In that basin the Lower Paleocene shoreface sandstone foresets of the Klitterhorn member of the Sediment Bjerge Formation are unconformably overlaid by fluvial sandstones of the Schjelderup member of the Vandfaldsdalen Formation (Larsen and Saunders, 1999; Larsen et al., 1999; Larsen et al., 2005; Larsen et al., 2016). In a recent paper Gerlings et al. (2017) correlated the metasedimentary sequence from LEG 152 to Aptian sediments dragged offshore Ammassalik representing the Mesozoic Ammassalik Basin to which they estimated a thickness of ca. 2 seconds (two-way time). The same sequence is suggested to be part of a wider area linked with the Hatton Bank-Rockall Plateau by Hitchen (2004).

In this paper we question the simple correlation between the metamorphic sequence and the Cretaceous succession indicating that the meta-volcaniclastic rocks belong to a Neoproterozoic sedimentary cycle possibly extending the Torridon basin of the Hebridean Foreland offshore South-East Greenland.

2. Method

2.a. Core sampling

The ODP Leg 152 site 917 is located on the South-East Greenland shelf approximately 50 Km offshore. The drill penetrated 821 m of Paleogene plateau basalts before reaching a thin layer (821.1 to 821.2 meters below sea bottom) of coarse-grained, quartz-rich sandstone of possible fluviatile origin, and of unknown age. Beneath this sandstone, steeply inclined, low-grade metamorphic rocks were encountered at 821.2 to 874.9 (mbsb). Core 103R corresponds to the topmost part of the metasedimentary succession reached at a depth of 826.9 down to 831.5 (mbsb), while core 110R represents the bottommost part between 865.3-874.9 (mbsb). Four samples were selected for Ar/Ar dating from core 917A and provided by the ODP repository in Bremen. These are 103R: 80-115 cm, 104R: 62-98 cm, 108R: 44-91 cm and 110R: 22-80 cm (Fig. 2). For those samples were also prepared thin sections for petrographic analysis because previous work by Vallier et al. (1998) indicated the presence of volcanic glass and plagioclase minerals replaced by secondary minerals. Finally, sample 103R was selected for automate quantitative mineral mapping (SEM) to spot minerals for U/Pd dating that were too small for hand picking.

2.b. Automated quantitative mineral mapping (AQM)

Automated quantitative mineral mapping (AQM) of sample 103R was performed at GEUS on a ZEISS Sigma 300VP Field Emission Scanning Electron Microscope (SEM) using the ZEISS Mineralogic software platform. The analysis was carried out under low vacuum (VP) conditions with an acceleration voltage of 15 kV, a 120 μm^2 aperture, a beam current of ca. 80 µA, and with 0.15 s dwell time. For further details about the AQM and the setup in ZEISS Mineralogic see Keulen et al (2020). An area of approximately 9x8 mm covering the location of the Ar/Ar dating spot site was selected for the analysis to characterize the bulk mineralogy of the sample and to screen for U/Pb dateable mineral phases. To increase resolution and to detect smaller grains, a step size between EDS analysis points of 5 µm was chosen. The AQM mineralogic results is presented in area% and not wt% as this would require more precise measurements of the phase chemistry.

2.c. U/Pb dating

U/Pb geochronology on apatite was carried out by laser ablation inductively coupled plasma mass spectrometry (LA-ICPMS) at GEUS. The U/Pb dating were performed in-situ on the same polished rock chip of sample 103R as for the Ar/Ar dating. Based on the AQM screening analysis, apatite mineral grains of preferably > 20 um in size were selected for the LA-ICPMS dating. The location of each apatite mineral grain as identified by the AQM and BSE images were transferred to the LA-ICPMS instrument by using a linear transformation matrix from the two coordinated frames, using six reference points, and thereby matching the position between the three (AQM + BSE images and LA-ICPMS instrument). A NWR 213 frequency-quintupled solid state Nd:YAG laser system from Elemental Scientific Lasers (ESL) mounted with a standard TV2 ablation cell was coupled to an ELEMENT 2 double-focusing single-collector magnetic sector-field ICPMS from Thermo-Fisher Scientific. The mass spectrometer is equipped with a new jet interface pump system, a detector amplifier, and employed Ni jet-type sampler and standard H-type skimmer cones. Operating conditions and data acquisition parameters are listed in Appendix 1. Prior to loading, the chip section and standards were carefully cleaned with ethanol to remove possible surface contamination. To ensure stable laser output energy, the laser was heated prior to operation, providing a stable laser power and flat ablation craters. The mass spectrometer was run for at least one hour before analysis to stabilize the background signal. The ablated material was swept by the helium carrier gas and mixed with argon gas ca. 0.5 m before entering the mass spectrometer. The ICP-MS was optimized for dry plasma conditions through continuous linear ablation of the GJ-1 zircon standard. The signal-to-noise ratios for the heavy mass range of interest (i.e. 202Hg to 238U), emphasizing on 238U and 206Pb, were maximized, while simultaneously opting for the lowest element-oxide production level by minimizing the UO2/U ratio. To minimize instrumental drift, a standard-sample-standard analysis protocol was followed, bracketing 7-8 samples by 4 standard measurements for each bracket. Standard analyses and results were validated by analyses of the natural apatite standards McClure (Schoene and Bowring 2006) and Durango (Chew et al. 2011), and the Plešovice (Slama et al. 2008) and GJ-1 (Jackson et al. 2004) zircon standards. All standards demonstrated an averaged age accuracy within 3% deviation (2σ) from reference values, and internal uncertainties of < 2-3% (2σ). Data processing was performed off-line using the software Iolite v. 2.5 (Paton et al. 2010, 2011) with the VizualAge data reduction scheme (Petrus & Kamber 2012). Data were corrected for background, session drift and down-hole isotopic fractionation by using GJ-1 as the primary reference material. Data was acquired from single spot analysis using a laser spot size of for the analyses of 25 µm. A laser fluence of ca. 3 J/cm^2 and a pulse rate of 5 Hz was applied. Acquisition sequence included 30 s background measurement, then laser ablation on for 40 s, and finally washout for 40 s. Factory-supplied software was used for the acquisition of the transient data, obtained through automated running mode of pre-set analytical locations.

Apatite usually require common Pb correction. However, for apatites with a high proportion of common Pb, assumption that the common Pb ratio is invariant will mean that any error in the isotope ratios assigned to common Pb will result in a consistent bias, rather than a random, of the calculated 206Pb/238U and 207Pb/206Pb radiogenic ratios (Ludwig, 1998). Thus, using a ‘‘SemiTotal–Pb/U isochron’’ approach (Tera and Wasserburg, 1972), the background- and session-drift corrected ratios can be plotted on the Tera-Wasserburg concordia diagram without correction for common Pb. If (and only if) the true 206Pb/238U and 207Pb/206Pb radiogenic isotope ratios represent comparable dates, the non-common Pb corrected data will be dispersed along a line whose lower intercept with the concordia curve defines the age of the episode responsible for this line (Ludwig, 1998). This is the case for the apatite grains herein, and thus the lower intercept age reported here for the apatites is not corrected for common Pb, assuming that this intercept age denotes the U/Pb isotopic age of a specific geological event recorded by the apatite mineral grains. Diagrams and statistical information were produced through the software IsoplotR (Vermeesch 2018).

2.d. $^{40}Ar/^{39}Ar$ dating

For $^{40}Ar/^{39}Ar$ age determination whole-rock mini-cores and biotite crystal separates were loaded into pits in aluminum irradiation disks. Each unknown was surrounded the neutron flux monitor Fish Canyon sanidine (FCs) with an assigned age of 28.201 (Kuiper et al., 2008).

The irradiation disks were then wrapped in aluminum foil and encapsulated in a heat-sealed quartz glass tube. The samples were irradiated in the cadmium-lined in-core (CLICIT) facility at the Oregon State University TRIGA reactor for 9 hours. Argon isotopic analyses of the gas released by laser step-heating of the whole-rock mini-cores and biotite separates (Supplementary data) were made on a fully automated, high-resolution Nu Instruments Noblesse multi-collector noble-gas mass spectrometer (Nu Instruments) at the Natural History Museum of Denmark, using previously documented instrumentation and procedures (Storey et al., 2007, Rivera et al., 2011). The data are reported relative to the astronomically calibrated $^{40}Ar/^{39}Ar$ age of 28.201 Ma for the Fish Canyon sanidine monitor mineral (Kuiper et al., 2008)).

3. Results

3.a. Petrography of the core samples

Representative optical microscopy images of thin section for the samples 103R, 104R, 108R and 110R are shown on Figure 3. As described by Vallier et al (1998), the mineral assemblages of all 4 samples are characteristic of the greenschist metamorphic facies, and the description given by Vallier et al (1998) is generally in accordance with our observations herein. The major mineral phases identified are chlorite that is omnipresent, white mica occurring exclusively as sericite, altered plagioclase feldspar (to chlorite, quartz, secondary feldspar, epidote and sericite), actinolite (from altered amphibole or pyroxene?), quartz, and epidote, with subordinate biotite, leucoxene, and Ti-oxides (most probably brookite or anatase). In addition, colorless, subhedral apatite (< 1 modal%) was identified in sample 103R, which is also the rock sample that contains 0.51 wt% P_2O_5. (Vallier et al, 1998). As described by Vallier et al (1998) recrystallization and metamorphic alteration has destroyed the original mineralogy and most original features. However, pseudomorphs after plagioclase feldspar laths in what resembles ophitic texture is observed in the samples 103R, 108R and 110R (Fig. 3A, C and D). In sample 103R and 108R, the laths are as large as 1 mm in length, and whereas in 108R the habitus of the laths are well defined (Fig. 3C), they appear more subhedral in sample 103R, in particular when occurring adjacent to the micro-crystalline "pseudomorph" domains that most probably has replaced glass matrix (Fig. 3A). This indicates a volcanic origin for especially the sample 103R (laths and glass) and

Thin-layered bedding dominated by quartz and subordinate feldspar and chlorite was observed in sample 104R and 110R (Fig. 3B, D). Small veins composed of primarily quartz with subordinate albite, chlorite and anhedral epidote was recognized in sample 103R only. Most epidote, though, appears in irregular, separate enclaves together with leucoxene and quartz. Titanite was not identified in any of the samples. Brown, pleochroic biotite occurs as a minor component (varies from <<1 % to a few modal%) in all four samples. In samples 104R and 108R occurrences of small, spherical structures of up to 200 μm in size and composed of a core of chlorite+quartz and with a rim of mainly feldspar with bluish 2. order interferences colors are observed. These structures were in Vallier et al (1998) interpretated as the original presence of radiolarians, thus being sedimentary structures. However, the resemblance to gas vesicles and thus micro-amygdules cannot be rules out.

3.b. Automated quantitative mineral mapping

The sample 103R is dominated by two main mineral phases, viz. chlorite/clinochlore and a phase characterized as "weathered amphibole", which corresponds to actinolite + various alteration overprints. Together, these phases cover ca. 88% of the sample area of sample 103R (Fig. 4). Quartz and Ti-oxides (most probably brookite, anatase, or leucoxene) cover ca. 2 area%, and all other phases <0.5 area% each. Apatite makes up circa 0.4 area% of the sample, and in general vary in mineral grain size according to the location of the apatites in the irregularly developed bedding that can be identified from the AQM image.

3.c. Apatite U/Pb dating

Uncertainty ellipses of the 25 individual spot analyses displayed in the Tera-Wasserburg Concordia (Fig. 5) are in 2σ level (Table 1). As the aim was to estimate a date for the deposition of the meta-volcaniclastic rocks, analytical procedures were optimized for single analysis of these small apatite grains. The unanchored lower intercept date of 905 +/- 21 Ma is reasonably well constrained with a MSWD = 1.6 due to a large spread in the radiogenic to common-Pb ratios, thus represent a robust age.

3.d. $^{40}Ar/^{39}Ar$ dating

Laser step-heating $^{40}Ar/^{39}Ar$ experiments were carried out on chloritized and rare, ~1-2 mm detrital biotite crystals found in core intervals 104R: 65-100 cm, 108R: 44-91 cm and 110R: 22-80 cm. Biotite crystals large enough for $^{40}Ar/^{39}Ar$ dating were not found in the uppermost of the 4 samples examined in this study (103R: 80-115 cm). In addition to the biotite analyses, $^{40}Ar/^{39}Ar$ experiments were also carried on ~2 mm diameter whole-rock mini-cores of all four samples obtained using a Dremmel rotary tool. Argon isotopic abundances, including the apparent ages of the individual steps and J-values, are given in Table 2 while step-heating plots are presented in Appendix 1.

Biotite

Depending on the gas yield, the laser step-heating $^{40}Ar/^{39}Ar$ experiments on single grain biotite were carried out in 2-3 steps, with the final step resulting in melting and complete outgassing of the grain. All the experiments gave Paleoproterozoic ages, with the youngest ages being typically associated with the first, low-power, laser step suggesting minor loss of radiogenic argon ($^{40}Ar^*$) due to alteration. Of the ten single grain experiments carried out, 5 yielded 2-step concordant ages and these are shown in Figure 2. These less isotopically disturbed grains indicate biotite crystallization/resetting semi-quantitative ages of around 1950 to 1850 Ma. The relatively small yield of 40Ar and low precision for these biotite analyses is indicative that they have suffered K loss by chloritization.

Whole-rock mini-cores

Detailed $^{40}Ar/^{39}Ar$ laser step heating experiments on 4 whole-rock mini-cores were carried out in order to investigate the provenance of the bulk meta-sediment as well as the age of the possible volcaniclastic unit represented by103R: 80-115 cm.

At lower laser power settings, the whole-rock mini-cores from 104R: 65-100 cm and 110R: 22-80 cm both yielded a staircase shaped pattern consistent with low temperature loss of ^{40}Ar. Increasing laser power gave Paleoproterozic ages but failed accepted statistical tests for an age plateau. Nonetheless, the range of ages yielded by these higher temperature steps is similar to the single crystal biotite $^{40}Ar/^{39}Ar$ data and suggests a single provenance for the bulk sediment for these samples.

In contrast to the stair-case shaped age spectra of the mini-cores from 104R: 65-100 cm and 110R: 22-80, the laser step-heating gas release patterns for the 2 mini-cores of the topmost, possible volcaniclastic, sample (917A-103R-85-115) yielded distinctive "U" shaped age profiles with minimum (Neoproterozoic) values for intermediate laser power steps (Fig. 6A). Both are also notable for having much higher Ca/K ratios when compared to data from the other mini-cores (Appendix 1) consistent with the presence of a compositionally distinct volcaniclastic component. The second of the two mini-cores analyzed from this sample produced a robust age plateau of 840 ± 50 Ma (MSWD = 0.64, p = 0.74) comprising 8 individual heating steps and 60% of the total ^{39}Ar released. These 8 steps yield an isochron age of 820 ± 40 Ma with a $^{40}Ar/^{36}Ar$ intercept of 410 ± 150 (Fig. 6B) which is within uncertainty of the atmospheric value of 298.56 (Lee et al., 2006). The isochron provides a minimum (Neoproterozoic) age for this potential meta-tuff layer in the upper part of Hole 917A.

4. Discussion and conclusion

The whole-rock mini-cores and chloritized biotite single crystal $^{40}Ar/^{39}Ar$ ages give semi-quantitative Paleoproterozoic ages from the lower samples and a robust Neoproterozoic isochron age from the top ones (Fig. 2). Here we explore whether the much younger age of 820 ± 40 Ma given by the mini-core from 103R-85-115 is the result of a partial reset due to the contact metamorphism of an overlying olivine-phyric basalt flow that were emplaced at ca. 1180 °C in subaerial conditions. In the Kangerlussuaq Basin, which is suggested to be the analogue for Core 917A (Larsen et al., 1994; Vallier et al., 1998), the only contact metamorphism documented is restricted to narrow zones close to the base of the lava flows, and the diagenetic processes in the entire sedimentary basin were enhanced by deep burial due to the thick pile of basalts of the Blosseville Group (Larsen et al. 2016). Other evidences that exclude the overprint of the Paleogene magmatism are: (1) the absence of thermal effects in the quartz-rich sandstone including unaltered micas that was recovered between the basalts and the meta-volcaniclastic rocks; (2) the chlorite geothermometer (Vallier et al., 1998) yielding average temperatures of 296°C for the top interval 103R, 300°C for interval 104R and 356°C for interval 108R at the bottom, thus showing no increase of temperature toward the contact with basaltic rocks (Fig. 2); (3) the distribution and chemistry of zeolites and clay minerals in the basalts from Core 917A (Demant et al. 1998) established that the mineralogical assemblages indicate a temperature of the metamorphism below 170°C and the zeolites formed during hydrothermal processes as late post-emplacement event affecting the whole volcanic pile (Fig. 2); (4) apatite fission tracks from interlava sediments of Leg 152 from Sites 914 and 915 (Clift et al. 1996) located on the continental shelf, and Site 918 that lies on oceanic crust of the Irminger Basin (Fig. 1) established that the central ages are significantly older (ca. 231 Ma to 150 Ma) than sample depositional ages (42 to 22 Ma). This implies that the samples did not experience significant post-depositional annealing (i.e. T > 110°C), and thus the temperature in the clastic rocks intercalated with the Paleogene basalts were never above 60°C, in agreement with the zeolites zonation.

For the abovementioned reasons we believe that the thermal heating irradiating from the Paleogene magmatism is quite unlikely and thus can be excluded. The greenschist facies metamorphism should then be older and not Cretaceous as it was assumed before. The same conclusion is valid for the supposed Cretaceous age of the meta-volcaniclastic rocks off-shore SE-Greenland that is now shown to be Neoproterozoic bracketed between 905 Ma and 820 Ma. The slightly younger whole-rock $^{40}Ar/^{39}Ar$ tuff age is consistent with low-temperature greenschist alteration of volcanic glass and secondary mineral growth (e.g. Verati and Jordan, 2014) presumably as a result of sedimentary burial in an extensional regime. The burial temperature was not sufficiently high, however, to significantly reset detrital and partly chloritized biotite from deeper in the sequence as these consistently give, all be it semi-quantitatively, Paleoproterozoic ages of around 1.9 to 1.8 Ga. All samples show that they were mainly composed of plagioclase feldspar grains, now replaced by albite and/or chlorite while other beds consist of irregular rock fragments now replaced by albite, chlorite, and quartz. These beds may have been lithic tuffs, consisting originally of plagioclase, volcanic glass, and volcanic rock fragments and ovoid quartz/albite masses in some thin sections, flattened parallel to bedding, may be replaced by vesicular volcanic glass, as also indicated by Vallier et al. (1998).

The absence of tectonic fabric together with the low-grade metamorphism could indicate that the thermal alteration is probably due to sedimentary burial during extensional tectonics as also suggested by Vallier et al. (1998) at 820±40 Ma, establishing the minimum age for the volcaniclastic succession.

The 905±21 Ma U/Pb age obtained from apatites in the tuff layer of core 917A allows possible correlations with Neoproterozoic successions across the North Atlantic and even though the data are limited only to this sample, this could potentially be equivalent to the Torridon Group succession in the Hebridean Foreland of the Scottish Caledonides (Fig. 7). Turnbull et al. (1996) obtained Rb-Sr data from analyses of whole-rock shale samples for the Diabaig Formation (994 ± 48 Ma) and for the Applecross Formation (977 ± 32 Ma) and interpreted as the time of albitization and clay conversion. These dates, which agree well with palaeomagnetic estimates, are interpreted as the time of early diagenesis which is probably within error of the time of deposition of the Torridon Group (Turnbull et al., 1996). Volcanic rocks of Torridonian age are rare in Scotland and volcanic deposits known from eastern Laurentia have a slight older age between 1300-1100 Ma (Batchelor 2011). The discovery of a crystal tuff in the Stoer Group (Batchelor and Prave 2010) established the earliest example so far of tholeiitic volcanic activity within the Torridonian of Scotland around 1187±35 Ma (Kinnaird et al., 2007). The calc-alkaline nature of the meta-volcaniclastic rocks in core 917A (Vallier et al., 1998) and the 905±21 Ma age of the tuff layer could indicate a correlative connection between the sedimentary basin offshore South-East Greenland and the 915±18 Ma magmatism associated with the Renlandian event (Leslie and Nutman 2003) of the Valhalla Orogeny (Cawood et al., 2010) or the volcanism/metamorphism in the West Highland domain of the Scottish Caledonides (Fig. 7). In any case the new data presented in this paper show for the first time the evidence for a Neoproterozoic sedimentary basin offshore South-East Greenland extending the foreland basins of the Scottish Caledonides to the conjugate margin also giving new insights for the interpretation of sedimentary basins below Tertiary basalts offshore Ammassalik and Rockall Plateau.

Acknowledgments

This study is part of the FINGERSEG project funded by Geocenter Denmark 2017 (P.I. Guarnieri P.). This paper is published under the agreement of the Geological Survey of Denmark and Greenland. We would like to thank Walter Hale form the Bremen Core Repository of the IODP for the samples provided and Daniel Wielandt for technical assistance with the $^{40}Ar/^{39}Ar$ analyses, as well as Mojgan Alaei, GEUS, for laboratory assistance. Quadlab is funded by the Villum Foundation.

Declaration of Interest

The authors have no conflict of interest.

References

Batchelor, R.A., 2011. Geochemistry of Torridonian tuffs and contemporary phosphorites:
potential for correlation of Torridonian sequences in NW Scotland. Scottish Journal of Geology 47, (2), 133–142

Batchelor, R.A., and Prave, A.R., 2010. Crystal tuff in the Stoer Group, Torridonian Supergroup, NW Scotland. Scottish Journal of Geology, 46/1, 1-6.

Cawood, P.A., Strachan, R., Cutts, K., Kinny, P.D., Hand, M., Pisarevsky, S., 2010. Neoproterozoic orogeny along the margin of Rodinia: Valhalla orogen, North Atlantic. Geology 38, 99-102.

Chew, D.M., Sylvester, P.J., Tubrett, M.N., 2011. U-Pb and Th-Pb dating of apatite by LA-ICPMS. Chemical Geology 280(1-7), 200-216.

Demant, A., Münch, P., Romeuf, N., and Morata, D., 1998. Distribution and chemistry of secondary minerals (zeolites and clay minerals) from Hole 917A, Southeast Greenland margin. In Saunders, A.D., Larsen, H.C., and Wise, S.W., Jr. (Eds.), Proceedings of the Ocean Drilling Program, Scientific Results, Vol. 152, 417-424.

Friend, C.R.L., Kinny, P.D., Rogers, G., Strachan, R.A. & Paterson, B.A., 1997. U–Pb zircon geochronological evidence for Neoproterozoic events in the Glenfinnan Group (Moine Supergroup): the formation of the Ardgour granite gneiss, north-west Scotland. Contributions to Mineralogy and Petrology, 128, 101–113.

Gerlings, J., Hopper, R.J., Fyhn, M.B.W., and Frandsen, N., 2017. Mesozoic and older rift basins on the SE Greenland Shelf offshore Ammassalik. In Péron-Pinvidic, G., Hopper, J. R., Stoker, M. S., Gaina, C., Doornenbal, J. C., Funck, T. & Árting, U. E. (eds). The NE Atlantic Region: A Reappraisal of Crustal Structure, Tectonostratigraphy and Magmatic Evolution. Geological Society, London, Special Publications, 447, 375–392.

Hitchen, K., 2004. The geology of the UK Hatton– Rockall margin. Marine and Petroleum Geology, 21, 993–1012.

Hopper, J.R., Funck, T., Stoker, M., Árting, U., Peron-Pindivic, G., Gaina, C. and Doornenbal, H., (eds) 2014. Tectonostratigraphic Atlas of the North-East Atlantic Region. Geological Survey of Denmark and Greenland (GEUS), Copenhagen.

Keulen, N., Malkki, S.N., Graham, S., 2020. Automated Quantitative Mineralogy Applied to Metamorphic Rocks: Minerals, 2020, 10 (1):47. https://doi.org/10.3390/min10010047.

Kinnaird, T.C., Prave, A.R., Kirkland, C.L., Horstwood, M., Parrish, R., and Batchelor, R. A., 2007. The late Mesoproterozoic–early Neoproterozoic tectonostratigraphic evolution of NW Scotland: the Torridonian revisited: Journal of the Geological Society, London, Vol. 164, 2007, pp. 541–551.

Kolb, J., 2014. Structure of the Palaeoproterozoic Nagssugtoqidian Orogen, SE Greenland: model for the tectonic evolution. Precambrian Research, 225, 809–822.

Kuiper, K.F., Deino A., Hilgen, F.J., Krijgsman, W., Renne, P.R., Wijbrans, J.R., 2008. Synchronizing rock clocks of Earth history Science 320 (5875), 500-504

Larsen, H.C., Saunders, A.D., Clift, P.D., and Shipboard Scientific Party, 1994. Proceedings of the Ocean Drilling Program, Initial Reports, Vol. 152, College Station, TX (Ocean Drilling Program).

Larsen, H.C., and Saunders, A.D., 1998. Tectonism and volcanism at the southeast Greenland rifted margin: a record of plume impact and later continental rupture. In: Saunders, A.D., Larsen, H.C. & Wise, S.W., JR. (eds) Proceedings of the Ocean Drilling Program, Scientific Results, Volume 152. Ocean Drilling Program, College Station, TX, 503–533.

Larsen, M., Hamberg, L., Olaussen, S., Nørgaard-Pedersen, N. and Stemmerik, L., 1999. Basin evolution in southern East Greenland: an outcrop analogue for Cretaceous – Paleogene basins in the North Atlantic volcanic margins. American Association of Petroleum Geologists Bulletin, 83, 1236– 1261.

Larsen, M., Bell, B., Guarnieri, P., Vosgerau, P., Weibel, R., 2018. Exploration challenges along the North Atlantic volcanic margins: the intra-volcanic sandstone play in subsurface and outcrop. Geological Society, London, Petroleum Geology Conference series 8, 231-245.

Lee, J.-Y., Marti, K., Severinghaus, J.P., Kawamura, K., Yoo, H.-S., Lee, J.B., Kim, J.S., 2006. A redetermination of the isotopic abundances of atmospheric Ar. Geochimica et Cosmochimica Acta 70, 4507–4512]

Leslie A.G., and Nutman A.P., 2003. Evidence for Neoproterozoic orogenesis and early high temperature Scandian deformation events in the southern East Greenland Caledonides. Geological Magazine 140 (3), 2003, pp. 309–333.

Millar, I.L., 1999. Neoproterozoic extensional basic magmatism associated with the West Highland granite gneiss in the Moine Supergroup of NW Scotland. Journal of the Geological Society, London, 156, 1153–1162.

Nielsen, T.F.D., Soper, N.J., Brooks, C.K., Faller, A.M., Higgins, A.C. & Matthews, D.W., 1981. The Pre-Basaltic Sediments and the Lower Basalts at Kangerdlugssuaq, East

Greenland: Their Stratigraphy, Lithology, Palaeomagnetism and Petrology. Meddelelser om Grønland Geoscience, 6.

Rivera, T.A, Storey, M., Zeeden C., Hilgen, F.J., Kuiper, K., 2011. A refined astronomically calibrated 40Ar/39Ar age for Fish Canyon sanidine. Earth and Planetary Science Letters 311 (3–4) 420–426.

Schoene, B., Bowring, S., 2006. U-Pb systematics of the McClure Mountain syenite: thermochronological constraints on the age of the 40Ar/39Ar standard MMhb. Contributions to Mineralogy and Petrology 151, 615-630.

Soper, N.J., Higgins, A.C., Matthews, D.W. & Brown, P.E. 1976. Late Cretaceous – early Tertiary stratigraphy of the Kangerdlugssuaq area, east Greenland, and the age of the opening of the north-east Atlantic. Journal of the Geological Society, London, 132, 85–104.

Storey, M., Duncan, R.A., Swisher, C.C., 2007. Paleocene-Eocene thermal maximum and the opening of the northeast Atlantic. Science, 316, 587-589.

Spencer, C.J., Kirkland, C.L., Prave, A.R., Strachan, R.A., Pease, V., 2019. Crustal reworking and orogenic styles inferred from zircon Hf isotopes: Proterozoic examples from the North Atlantic region. Geoscience Frontiers, Volume 10, Issue 2, 417-424. https://doi.org/10.1016/j.gsf.2018.09.008.

Tegner, C., Duncan, R.A., Bernstein, S., Brooks, C.K., Bird, D.K. & Storey, M. 1998. Ar-40-Ar-39 geochronology of Tertiary mafic intrusions along the East Greenland rifted margin: relation to flood basalts and the Iceland hotspot track. Earth and Planetary Science Letters, 156, 75–88.

Turnbull, M.J.M., Whitehouse, M.J., Moorbath, S., 1996. New isotopic age determinations for the Torridonian, NW Scotland. Journal of the Geological Society of London 153, 955–964.

Vallier, T., Calk, L., Stax, R., and Demant, A., 1998. Metamorphosed sedimentary (volcaniclastic?) Rocks beneath Paleocene Basalt in Hole 917A, East Greenland margin. In Saunders, A.D., Larsen, H.C., and Wise, S.W., Jr. (Eds.), Proceedings of the Ocean Drilling Program, Scientific Results, Vol. 152, 129-144.

Verati C. and Jourdan F. 2014. Modelling effect of sericitization of plagioclase on the 40K/40Ar and 40Ar/39Ar chronometers: implication for dating basaltic rocks and mineral deposits Geological Society London Special Publications 378, 155-174.

Vermeesch, P., 2018. IsoplotR: A free and open toolbox for geochronology. Geoscience Frontiers 9, 1479-1493.

Figure captions

Figure 1. South-East Greenland and Rockall conjugate margins (with shaded relief bathymetry/topography as background) and distribution of the North Atlantic Igneous Province (modified after Hopper et al. 2014). The location of the ODP Leg-152 sites is also provided.

Figure 2. Condensed log summary for Site 917, bottom part of the Hole 917A (modified after Larsen et al., 1994). Zeolite zonation typical of very low-grade corresponds to temperatures less than 170°C (Demant et al. 1998). The temperature of equilibration of chlorite in the metasedimentary rocks of Hole 917A (after Vallier et al. 1998) increases downhole. $^{40}Ar/^{39}Ar$ age of the basalts (*) after Storey et al. 2007. Biotite $^{40}Ar/^{39}Ar$ concordant ages of the metavolcaniclastic rocks and U/Pb apatite age this study.

Figure 3. Optical microscopy images of the thin sections investigated in this study. (A) PPL of sample 103R showing pseudo-intersertal texture with subhedral pseudomorph laths after plagioclase in a microcrystalline matrix replacing most likely the original glass matrix. Further, the typical appearance of cross-cutting quartz veins and of apatite mineral grains. (B) XPL of sample 104R showing recrystallized original bedding with thin layers of mostly quartz interbedded with layers composed of predominantly chlorite, actinolite, sericite white mica, feldspar and leucoxene. (C) PPL of sample 108R with relatively large, anhedral pseudomorph laths after plagioclase feldspar in a metamorphic matrix composed of chlorite, actinolite, recrystallized feldspar, sericite white mica and leucoxene. (D) PPL of sample 110R showing the original bedding with a thin layer of mostly quartz as well as chlorite and feldspar surrounded by layers composed predominantly of chlorite, actinolite, sericite white mica, plagioclase feldspar pseudomorph laths, leucoxene, biotite and epidote.

Figure 4. Scanning Electron Microprobe mineral map. (A) Back scattered electron (BSE) map; (B) AQM mineral map with detailed inset.

Figure 5. Unanchored Tera-Wasserburg Concordia diagram for the apatite grains measured in this study. The regression line and corresponding uncertainty have been determined using model 2 of the IsoplotR as described in Vermeesch (2018).

Figure 6. $^{40}Ar/^{39}Ar$ step-heating (A) and isochron (B) plots for a mini-core from sample 103R-85-115 from ODP hole 152-917A. See text for further details.

Figure 7. Neoproterozoic paleogeographic reconstruction of Laurentia and Baltica (modified after Cawood et al., 2010; Spencer et al. 2019) showing the position of the meta-volcaniclastic rocks of site 917A compared to the Torridon Group in the Hebridean Foreland of the Scottish Caledonides that were depocenters for sediments derived from the Grenville and Valhalla orogens.

Tables

Table 1. U/Pb dating results.

Table 2. $^{40}Ar/^{39}Ar$ biotite and whole-rock mini-core laser step heating data.

Appendices

Appendix 1. Operating conditions for LA-ICPMS analysis.

Appendix 2. $^{40}Ar/^{39}Ar$ step-heating plots for biotite single crystals and mini-cores.

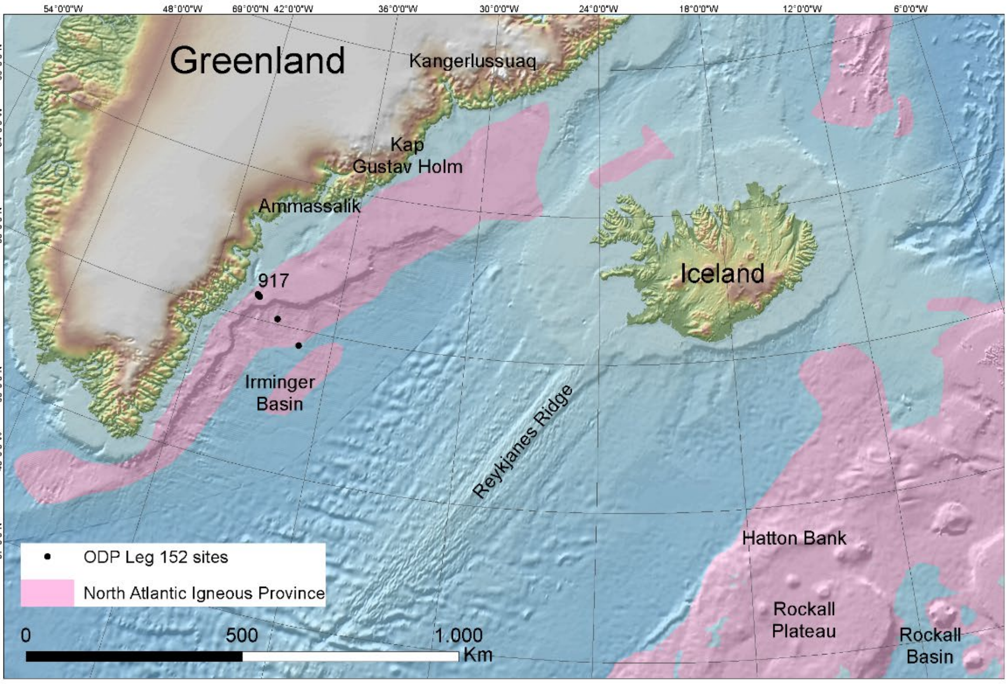

54°0'0"W
48°0'0"W
69°0'0"N
42°0'0"W
36°0'0"W
30°0'0"W
24°0'0"W
18°0'0"W
12°0'0"W
6°0'0"W
66°0'0"N
54°0'0"W
63°0'0"N
60°0'0"N
48°0'0"W
57°0'0"N
Greenland
Kangerlussuaq
Kap
Gustav Holm
Ammassalik
917
Iceland
Irminger
Basin
Reykjanes Ridge
Hatton Bank
Rockall
Plateau
Rockall
Basin
ODP Leg 152 sites
North Atlantic Igneous Province
0
500
1.000
Km

Fig. 1

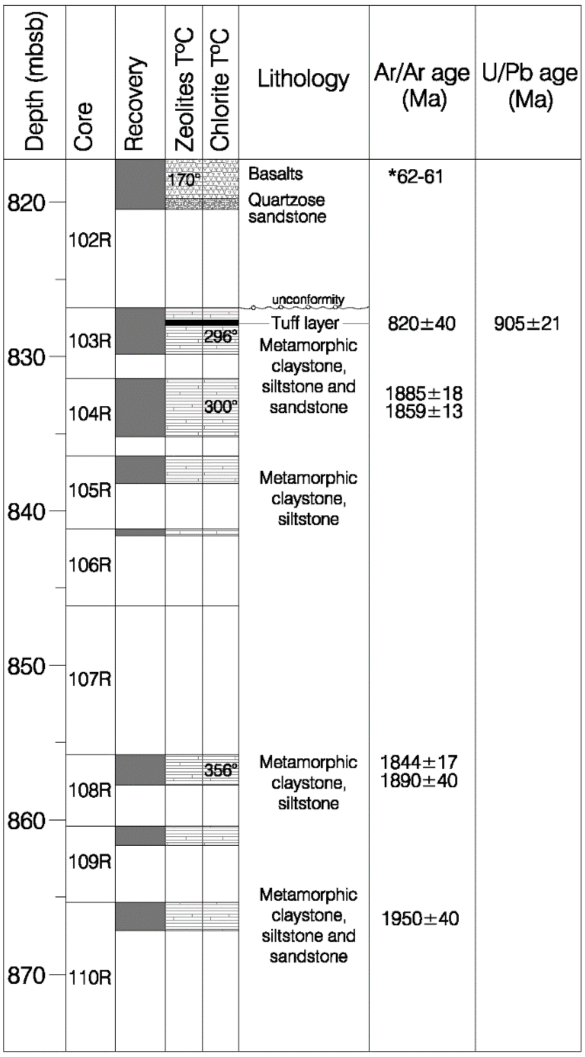
Depth (mbsb)
Core
Recovery
Zeolites T°C
Chlorite T°C
Lithology
Ar/Ar age (Ma)
U/Pb age (Ma)
820
830
840
850
860
870
102R
103R
104R
105R
106R
107R
108R
109R
110R
170°
296°
300°
356°
Basalts
Quartzose sandstone
unconformity
Tuff layer
Metamorphic claystone, siltstone and sandstone
Metamorphic claystone, siltstone
Metamorphic claystone, siltstone
Metamorphic claystone, siltstone and sandstone
*62-61
820±40
1885±18
1859±13
1844±17
1890±40
1950±40
905±21

Fig. 2

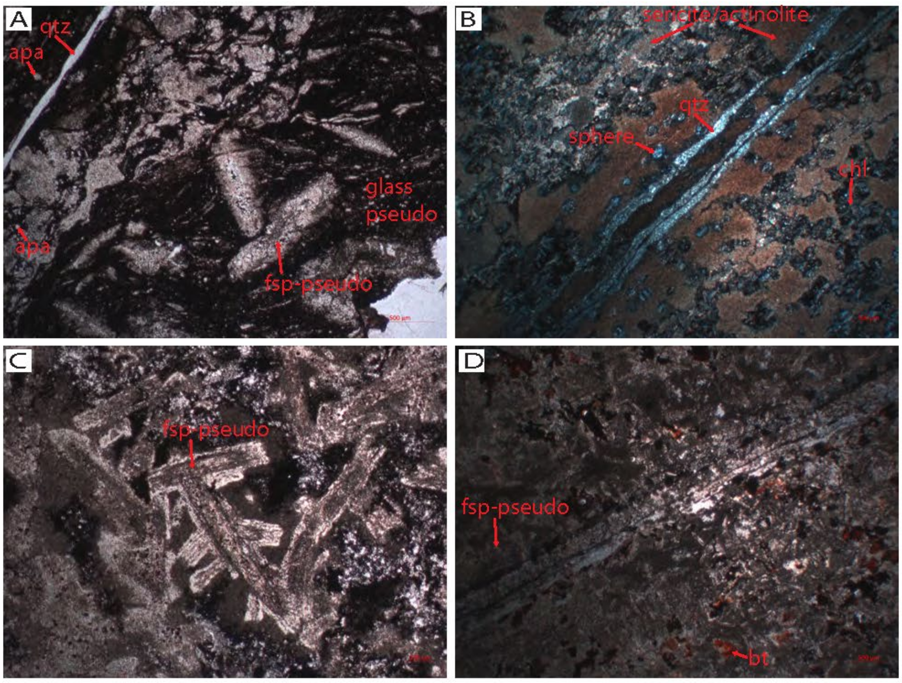
A
qtz
apa
glass
pseudo
apa
fsp-pseudo
B
sericite/actinolite
qtz
sphere
chl
C
fsp-pseudo
D
fsp-pseudo
bt

Fig. 3

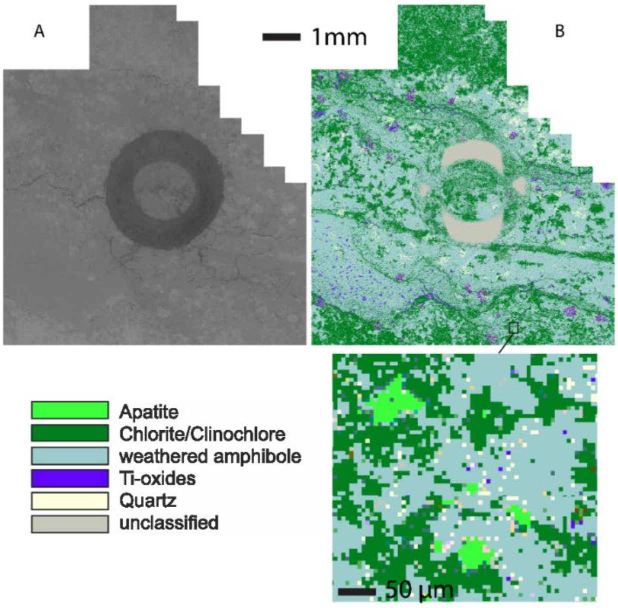
A
1mm
B
Apatite
Chlorite/Clinochlore
weathered amphibole
Ti-oxides
Quartz
unclassified
50 µm

Fig. 4

Fig. 5

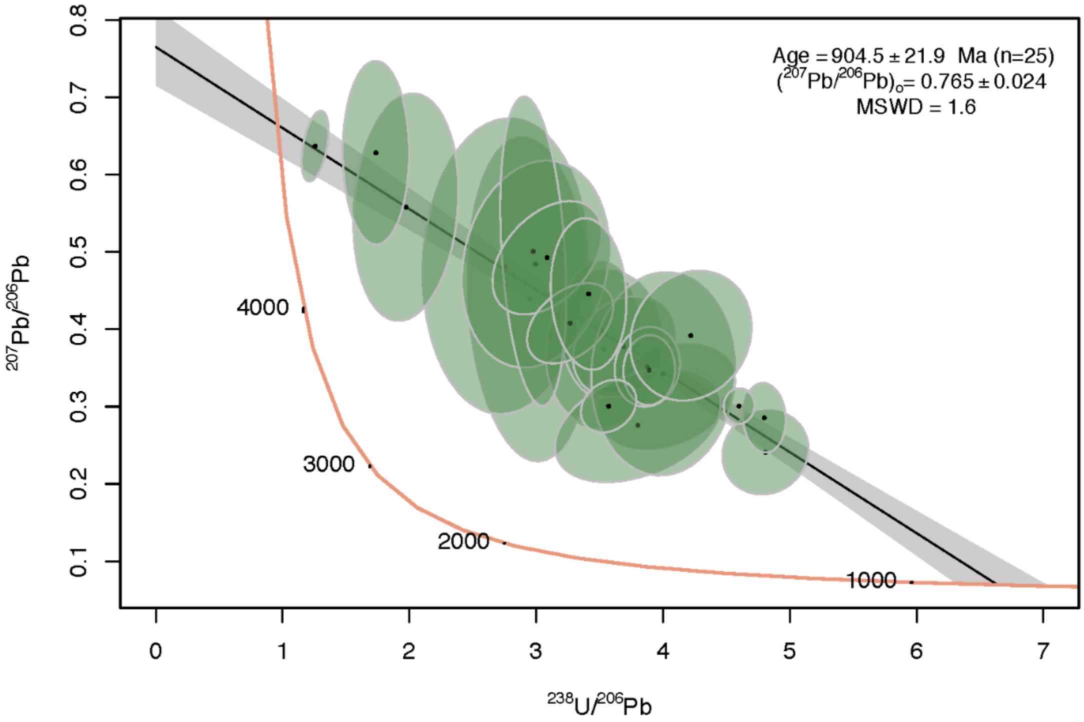
Age = 904.5 ± 21.9 Ma (n=25)
($^{207}Pb/^{206}Pb)_o$= 0.765 ± 0.024
MSWD = 1.6
4000
3000
2000
1000
$^{207}Pb/^{206}Pb$
$^{238}U/^{206}Pb$
0.1
0.2
0.3
0.4
0.5
0.6
0.7
0.8
0
1
2
3
4
5
6
7

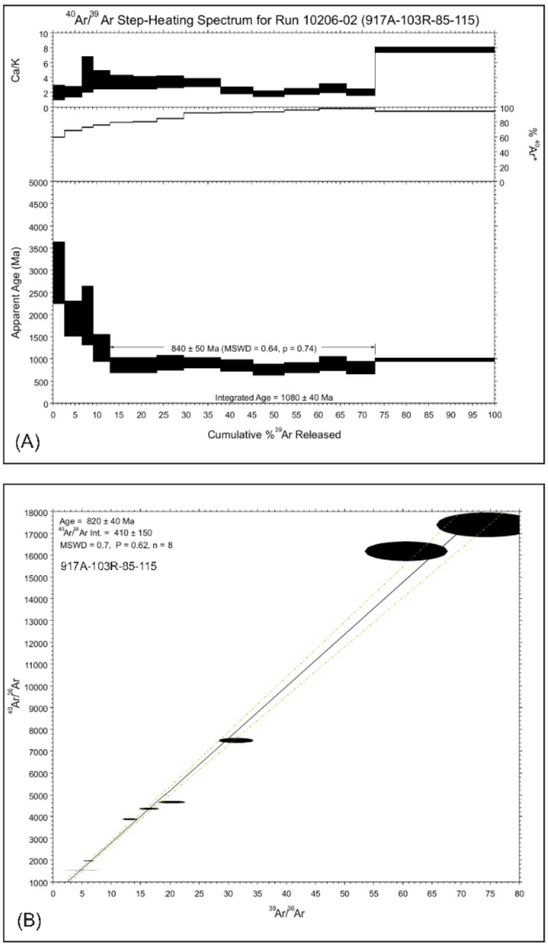
40Ar/39Ar Step-Heating Spectrum for Run 10206-02 (917A-103R-85-115)
Ca/K
% 40Ar*
Apparent Age (Ma)
840 ± 50 Ma (MSWD = 0.64, p = 0.74)
Integrated Age = 1080 ± 40 Ma
Cumulative %39Ar Released
(A)
Age = 820 ± 40 Ma
40Ar/36Ar Int. = 410 ± 150
MSWD = 0.7, P = 0.62, n = 8
917A-103R-85-115
40Ar/36Ar
39Ar/36Ar
(B)

(Fig. 6)


LAURENTIA
Valhalla Orogen
Ammassalik
ODP site 917A
Torridon
Group
Canada
Labrador
Grenville
Rockall Plateau
1000 km
BALTICA

Fig. 7

Sample	Analysis	CONCENTRATIONS[a]						RATIOS										AGES						CONCORDANCE	
		U [ppm]	2 σ	Th [ppm]	2 σ	Pb [ppm]	2 σ	U/Th[a]	$^{207}Pb/^{235}U$[b]	2 σ[d]	$^{206}Pb/^{238}U$[b]	2 σ[d]	rho[c]	$^{207}Pb/^{206}Pb$[e]	2 σ[d]	$^{208}Pb/^{232}Th$[e]	2 σ[d]	$^{207}Pb/^{235}U$[b]	2 σ[d]	$^{206}Pb/^{238}U$[b]	2 σ[d]	$^{207}Pb/^{206}Pb$[e]	2 σ[d]	Wetherill	Tera-Wasserburg
Output_1_2	Ap_sample-014.FIN2	1.32	0.3	1.24	0.26	2.7	0.98	1.022	10.7	1.9	0.248	0.027	0.59297	0.315	0.051	0.232	0.047	2460	190	1430	140	3490	260	58	41
Output_1_4	Ap_sample-021.FIN2	0.78	0.3	0.8	0.49	2.73	0.96	1.24	20.5	8.8	0.339	0.046	0.99614	0.43	0.14	0.46	0.27	3060	460	1880	220	3980	540	61	47
Output_1_8	Ap_sample-037.FIN2	0.81	0.6	0.91	0.9	3.6	3.1	1	24.1	8.9	0.363	0.07	0.99665	0.478	0.098	0.437	0.051	3230	410	1990	330	4160	320	62	48
Output_1_9	Ap_sample-039.FIN2	0.82	0.1	0.51	0.11	1.95	0.42	1.64	14.6	3.5	0.283	0.03	0.63181	0.377	0.078	0.421	0.072	2750	230	1600	150	3770	320	58	42
Output_1_10	Ap_sample-040.FIN2	0.79	0.2	0.64	0.15	2.05	0.47	1.25	15.7	3.1	0.285	0.021	0.96762	0.404	0.069	0.43	0.11	2830	200	1620	110	4010	150	57	40
Output_1_12	Ap_sample-049.FIN2	0.78	0.2	0.72	0.21	1.96	0.46	0.958	14.1	2.1	0.271	0.024	0.97967	0.383	0.069	0.285	0.021	2750	140	1550	120	3830	290	56	40
Output_1_13	Ap_sample-053.FIN2	1.45	0.6	1.14	0.45	3.5	2.1	1.1	10	2.1	0.263	0.037	0.72337	0.277	0.04	0.325	0.087	2390	200	1500	190	3300	230	63	45
Output_1_15	Ap_sample-060.FIN2	0.6	0.1	0.47	0.13	2.65	0.9	1.66	22.3	5.7	0.334	0.053	0.97819	0.485	0.079	0.65	0.22	3170	230	1850	260	4180	240	58	44
Output_1_16	Ap_sample-061.FIN2	0.63	0.1	0.86	0.3	2.26	0.98	1.06	11.8	3.9	0.25	0.029	0.86667	0.313	0.075	0.307	0.098	2500	320	1440	150	3440	410	58	42
Output_1_20	Ap_sample-065.FIN2	3.21	0.4	4.55	0.67	4.9	0.89	0.823	6.9	1.3	0.208	0.012	0.94398	0.225	0.038	0.127	0.022	2060	170	1219	65	3040	280	59	40
Output_1_21	Ap_sample-073.FIN2	7.24	0.5	56.4	3.8	20	1.8	0.133	8.2	1.1	0.2084	0.006	0.73345	0.278	0.027	0.0395	0.005	2240	110	1220	32	3380	160	54	36
Output_1_22	Ap_sample-074.FIN2	0.554	0.1	2.1	0.66	1.9	0.44	0.266	23.2	8.2	0.336	0.024	0.83573	0.46	0.13	0.095	0.048	3120	370	1870	120	3970	520	60	47
Output_1_24	Ap_sample-076.FIN2	2.8	1	5.5	1.5	10.3	3.9	0.426	12.5	1.6	0.258	0.014	0.79368	0.351	0.035	0.175	0.022	2630	130	1478	72	3690	150	56	40
Output_1_25	Ap_sample-078.FIN2	1.66	0.5	4.7	1.5	5.3	1.5	0.345	12.3	1.4	0.257	0.011	0.69617	0.346	0.034	0.13	0.011	2610	110	1471	57	3670	160	56	40
Output_1_26	Ap_sample-079.FIN2	0.72	0.1	2.07	0.86	2.66	0.37	0.39	22	2.8	0.324	0.037	0.09726	0.496	0.056	0.173	0.066	3170	120	1810	180	4210	180	57	43
Output_1_27	Ap_sample-085.FIN2	0.72	0.5	1.4	1.1	8.8	7.3	0.539	69.9	4.8	0.796	0.055	0.1461	0.639	0.059	0.709	0.037	4326	70	3770	200	4600	130	87	82
Output_1_28	Ap_sample-086.FIN2	0.79	0.2	2.2	0.45	5.2	2.5	0.355	39	10	0.507	0.087	0.90294	0.554	0.062	0.258	0.067	3720	240	2640	370	4380	160	71	60
Output_1_29	Ap_sample-087.FIN2	0.93	0.2	2.08	0.62	2.82	0.64	0.439	17.2	1.8	0.306	0.026	0.94709	0.411	0.069	0.155	0.034	2940	100	1720	130	3940	250	59	44
Output_1_30	Ap_sample-088.FIN2	1.28	0.3	3.41	0.92	2.81	0.77	0.36	12.8	2.4	0.237	0.022	0.79609	0.373	0.054	0.099	0.014	2630	180	1370	110	3760	220	52	36
Output_1_32	Ap_sample-090.FIN2	0.86	0.2	2.53	0.51	3.8	1	0.328	18	3.6	0.293	0.021	0.84035	0.445	0.079	0.166	0.012	2980	200	1650	100	4050	270	55	41
Output_1_36	Ap_sample-100.FIN2	0.89	0.2	1.28	0.15	3.6	1.2	0.81	16.5	3.6	0.297	0.044	0.92105	0.406	0.088	0.32	0.14	2890	230	1670	220	3900	330	58	43
Output_1_37	Ap_sample-101.FIN2	2.57	0.4	16	3.6	12	2.1	0.214	11.6	1.1	0.28	0.014	0.84195	0.307	0.017	0.1006	0.006	2565	85	1588	70	3501	90	62	45
Output_1_43	Ap_sample-128.FIN2	0.82	0.3	0.82	0.54	7.6	5.4	1.07	49.9	9.9	0.576	0.071	0.99341	0.627	0.051	1.01	0.15	3980	210	2930	290	4570	120	74	64
Output_1_4	Ap_sample-023.FIN2	0.76	0.2	1.15	0.21	1.33	0.55	0.697	7.3	2.7	0.229	0.032	0.79556	0.246	0.085	0.141	0.039	2130	440	1320	170	3060	550	62	43
Output_1_29	Ap_sample-090.FIN2	2.64	0.2	10.15	0.87	7.9	0.76	0.266	9.01	0.59	0.2174	0.0047	0.35254	0.297	0.018	0.0874	0.006	2338	61	1268	25	3452	95	54	37

[a]U, Th and Pb concentrations with errors (2SE) and U/Th ratios are calculated relative to the GJ-1 reference zircon
[b]Corrected for background, downhole and within-run Pb/U fractionation. Normalised to the reference zircon GJ-1 (TIMS/measured values). The $^{207}Pb/^{235}U$ is calculated through: $(^{207}Pb/^{206}Pb)/(^{238}U/^{206}Pb * 1/137.818)$
[c]Rho is the error correlation defined as the quotient of the propagated errors of the $^{206}Pb/^{238}U$ and $^{207/235}U$ ratios
[d]Quadratic addition of within-run errors (2 SE) and the all-session reproducibility of GJ-1 (2 SE)
[e]Normalised to the GJ-1 reference zircon (~0.6 per atomic mass unit)
[f]Common Pb correction through measured Pb^{204} (corrected for Hg^{204} using natural abundance Hg isotopic ratios) and the model Pb composition of Stacey & Kramers (1975)

Tab. 1.

Lab ID#	Laser	Relative Isotopic Abundances										Ca/K		$\%^{40}Ar^{*}$	Age (Ma)	
	Watts	^{40}Ar	±1σ	^{39}Ar	±1σ	^{38}Ar	±1σ	^{37}Ar	±1σ	^{36}Ar	±1σ		±1σ			±1σ
Single crystal biotite (bio)																
917A-104R-65-100_bio (J = 0.0023645 ± 0.0000042)																
10212-01A	1.0	65.100	0.004	0.0988	0.0012	0.00122	0.00001	0.00175	0.00066	0.000237	0.000007	0.035	0.013	99.9	1718	14
10212-01B	2.0	84.538	0.005	0.1118	0.0012	0.00137	0.00001	0.00030	0.00065	0.000054	0.000005	0.005	0.011	100.0	1876	13
10212-01C	2.5	29.728	0.003	0.0432	0.0012	0.00050	0.00001	0.00000	0.00060	0.000042	0.000005	0.000	0.027	100.0	1768	33
917A-104R-65-100_bio (J = 0.0023624 ± 0.0000027)																
10213-01A	1.0	72.027	0.004	0.1139	0.0013	0.00145	0.00001	0.00168	0.00069	0.000451	0.000008	0.029	0.012	99.8	1671	12
10213-01B	2.0	95.572	0.006	0.1224	0.0013	0.00144	0.00001	0.00015	0.00071	0.000093	0.000006	0.002	0.011	100.0	1913	12
10213-01C	2.5	35.517	0.004	0.0518	0.0012	0.00058	0.00001	0.00000	0.00054	0.000074	0.000005	0.000	0.020	99.9	1762	26
10213-02A	1.0	52.894	0.004	0.0814	0.0012	0.00114	0.00001	0.00129	0.00060	0.000594	0.000008	0.031	0.014	99.7	1699	17
10213-02B	2.0	127.122	0.006	0.1665	0.0013	0.00212	0.00001	0.00000	0.00062	0.000460	0.000008	0.000	0.007	99.9	1886	9
10213-02C	2.5	37.854	0.003	0.0499	0.0013	0.00064	0.00001	0.00000	0.00068	0.000208	0.000007	0.000	0.027	99.8	1876	30
10213-03B	2.0	166.803	0.007	0.2243	0.0014	0.00268	0.00001	0.00206	0.00056	0.000112	0.000006	0.018	0.005	100.0	1856	7
10213-03C	2.5	65.059	0.004	0.0858	0.0014	0.00106	0.00001	0.00000	0.00062	0.000071	0.000006	0.000	0.014	100.0	1878	19
10213-04A	1.0	71.547	0.005	0.1124	0.0012	0.00139	0.00001	0.00052	0.00060	0.000177	0.000007	0.009	0.010	99.9	1679	12
10213-04B	2.0	146.314	0.007	0.1913	0.0012	0.00226	0.00001	0.00000	0.00068	0.000078	0.000006	0.000	0.007	100.0	1889	7
10213-04C	2.5	43.861	0.004	0.0609	0.0013	0.00073	0.00001	0.00092	0.00069	0.000034	0.000005	0.030	0.022	100.0	1819	24
917A-108R-45-90_bio (J = 0.0023633 ± 0.0000021)																
10215-01A	1.0	146.932	0.008	0.1897	0.0014	0.00724	0.00003	0.01082	0.00088	0.024210	0.000047	0.112	0.009	95.1	1845	9
10215-01B	2.0	26.756	0.004	0.0356	0.0014	0.00110	0.00001	0.00028	0.00095	0.003620	0.000023	0.015	0.052	96.0	1820	45
10215-04A	1.0	11.226	0.003	0.0224	0.0012	0.00038	0.00001	0.00000	0.00065	0.000140	0.000005	0.000	0.057	99.6	1427	52
10215-04B	2.0	43.080	0.003	0.0574	0.0011	0.00073	0.00001	0.00003	0.00063	0.000056	0.000005	0.001	0.021	100.0	1866	23
10215-06A	1.0	19.162	0.003	0.0285	0.0013	0.00065	0.00001	0.00045	0.00062	0.001280	0.000011	0.031	0.043	98.0	1718	49
10215-06B	2.0	56.327	0.004	0.0731	0.0013	0.00096	0.00001	0.00131	0.00061	0.000078	0.000005	0.035	0.016	100.0	1898	21
10215-06C	2.5	19.494	0.003	0.0271	0.0014	0.00034	0.00001	0.00000	0.00066	0.000057	0.000005	0.000	0.048	99.9	1816	60
917A-110R-65-105_bio (J = 0.0023696 ± 0.0000039)																
10217-01A	1.0	9.676	0.002	0.0147	0.0012	0.00021	0.00000	0.00092	0.00066	0.000104	0.000006	0.123	0.089	99.7	1713	92
10217-01B	2.0	29.477	0.003	0.0367	0.0012	0.00046	0.00001	0.00000	0.00062	0.000078	0.000006	0.000	0.033	99.9	1950	39
10217-02A	1.0	19.543	0.003	0.0269	0.0012	0.00041	0.00001	0.00028	0.00081	0.000241	0.000006	0.020	0.059	99.6	1829	50
10217-02B	2.0	61.397	0.004	0.0766	0.0012	0.00105	0.00001	0.00303	0.00070	0.000127	0.000006	0.077	0.018	99.9	1947	19
10217-02C	2.5	11.665	0.002	0.0139	0.0012	0.00022	0.00001	0.00236	0.00070	0.000048	0.000005	0.333	0.103	99.9	2002	109
Whole-rock mini-cores (mc)																
917A-103R-85-115_mc (J = 0.0023786 ± 0.0000012)																
10206-01F	4.0	7.0522	0.0018	0.0062	0.0011	0.001910	0.000011	0.0110	0.0006	0.00891	0.00002	3.5	0.7	62.3	1809	212
10206-01G	4.5	4.5299	0.0016	0.0051	0.0012	0.001300	0.000009	0.0146	0.0005	0.004820	0.000020	5.6	1.3	68.3	1629	249
10206-01H	5.0	3.2559	0.0015	0.0041	0.0012	0.001180	0.000009	0.0179	0.0006	0.003110	0.000015	9	3	71.5	1575	325
10206-01I	5.5	2.6128	0.0016	0.0040	0.0012	0.001240	0.000010	0.0208	0.0006	0.002400	0.000014	10	3	72.6	1374	292
10206-01J	6.0	2.3685	0.0016	0.0047	0.0012	0.001420	0.000010	0.0233	0.0005	0.002240	0.000015	10	2	71.9	1148	219
10206-01K	6.5	2.2984	0.0016	0.0059	0.0012	0.001550	0.000012	0.0265	0.0007	0.002230	0.000014	8.8	1.8	71.1	930	147
10206-01L	7.0	2.3056	0.0016	0.0026	0.0012	0.001540	0.000012	0.0348	0.0009	0.002140	0.000016	26	12	72.4	1713	515
10206-01M	7.5	2.3906	0.0016	0.0031	0.0012	0.001510	0.000012	0.0373	0.0006	0.001880	0.000013	23	9	76.7	1606	406
10206-01N	8.0	2.3839	0.0016	0.0086	0.0011	0.001310	0.000010	0.0496	0.0008	0.001620	0.000011	11.3	1.5	79.9	775	83
10206-01O	8.5	2.3702	0.0017	0.0049	0.0012	0.000849	0.000008	0.0716	0.0009	0.001320	0.000011	29	7	83.7	1244	216
10206-01P	9.0	2.2477	0.0016	0.0081	0.0012	0.000522	0.000006	0.0849	0.0010	0.000996	0.000009	20	3	87.1	837	100
10206-01Q	10.0	2.2585	0.0016	0.0055	0.0011	0.000474	0.000006	0.1283	0.0012	0.001060	0.000010	45	9	86.5	1129	177
10206-01R	12.0	8.4115	0.0019	0.0240	0.0012	0.001610	0.000011	0.296	0.002	0.003320	0.000015	24.1	1.2	88.5	1017	38
10206-01fusior	20.0	7.1425	0.0016	0.0159	0.0012	0.001040	0.000010	0.1610	0.0018	0.002470	0.000015	19.9	1.5	89.9	1240	67
Note: Low-power laser degassing steps A to E had insignificant 39Ar																
917A-103R-85-115_mc (J = 0.0023786 ± 0.0000012)																
10206-02D	3.0	13.4572	0.0020	0.0048	0.0011	0.003550	0.000017	0.0048	0.0005	0.01820	0.00004	1.9	0.5	59.6	2931	346
10206-02E	3.5	7.8436	0.0016	0.0070	0.0012	0.001720	0.000012	0.0072	0.0005	0.00836	0.00003	2.0	0.4	68.2	1903	200
10206-02F	4.0	5.0587	0.0016	0.0045	0.0012	0.001110	0.000010	0.0100	0.0006	0.004640	0.000019	4.4	1.2	72.7	1976	331
10206-02G	4.5	3.7287	0.0015	0.0069	0.0012	0.000965	0.000008	0.0129	0.0006	0.003050	0.000015	3.7	0.6	75.6	1245	151
10206-02H	5.0	3.1987	0.0015	0.0089	0.0012	0.000969	0.000010	0.0153	0.0006	0.002360	0.000014	3.4	0.5	78.0	939	98
10206-02I	5.5	2.8714	0.0016	0.0091	0.0012	0.001010	0.000010	0.0155	0.0006	0.001990	0.000012	3.3	0.4	79.4	854	88
10206-02J	6.0	2.9554	0.0017	0.0096	0.0012	0.001070	0.000009	0.0161	0.0006	0.001950	0.000013	3.3	0.4	80.4	846	86
10206-02K	6.5	3.3353	0.0017	0.0105	0.0012	0.000917	0.000008	0.0179	0.0006	0.001710	0.000011	3.3	0.4	84.7	905	84
10206-02L	7.0	4.3365	0.0018	0.0149	0.0013	0.000560	0.000006	0.0247	0.0007	0.001120	0.000009	3.2	0.3	92.3	907	61
10206-02M	7.5	3.4280	0.0018	0.0130	0.0012	0.000362	0.000006	0.0148	0.0006	0.000792	0.000008	2.2	0.2	93.1	840	64
10206-02N	8.0	2.8689	0.0015	0.0126	0.0013	0.000321	0.000006	0.0115	0.0006	0.000620	0.000008	1.8	0.2	93.6	750	63
10206-02O	8.5	3.3497	0.0015	0.0141	0.0013	0.000329	0.000006	0.0150	0.0006	0.000452	0.000007	2.1	0.2	96.0	795	58
10206-02P	9.0	2.8975	0.0016	0.0109	0.0012	0.000199	0.000004	0.0139	0.0006	0.000183	0.000005	2.5	0.3	98.2	886	79
10206-02Q	10.0	2.6777	0.0016	0.0115	0.0013	0.000175	0.000004	0.0115	0.0006	0.000157	0.000005	2.0	0.2	98.3	798	71
10206-02fusior	20.0	15.021	0.002	0.0481	0.0012	0.001300	0.000010	0.1887	0.0013	0.002840	0.000015	7.69	0.19	94.4	975	18
Note: Low-power laser degassing steps A, B and C had insignificant 39Ar																
917A-104R-65-100_mc (J = 0.0023777 ± 0.0000013)																
10207-03A	2.0	14.915	0.002	0.0811	0.0015	0.004110	0.000019	0.0038	0.0004	0.01667	0.00004	0.092	0.011	66.6	468	8
10207-03B	3.0	47.308	0.004	0.1605	0.0015	0.003150	0.000016	0.0067	0.0004	0.00674	0.00002	0.082	0.006	95.7	940	7
10207-03C	4.0	108.363	0.008	0.2571	0.0015	0.003940	0.000016	0.0118	0.0005	0.004320	0.000018	0.090	0.004	98.8	1260	5
10207-03D	5.0	217.594	0.012	0.3902	0.0016	0.00526	0.00002	0.0189	0.0006	0.002320	0.000013	0.095	0.003	99.7	1542	4
10207-03E	5.5	317.583	0.017	0.4937	0.0015	0.00622	0.00002	0.0206	0.0006	0.001250	0.000010	0.082	0.002	99.9	1697	3

Tab. 2

Lab ID#	Laser	Relative Isotopic Abundances										Ca/K		%^{40}Ar*	Age (Ma)	
	Watts	^{40}Ar	±1σ	^{39}Ar	±1σ	^{38}Ar	±1σ	^{37}Ar	±1σ	^{36}Ar	±1σ	Ca/K	±1σ		Age (Ma)	±1σ
10207-03F	6.0	454.69	0.02	0.6598	0.0016	0.00802	0.00002	0.0255	0.0006	0.000969	0.000010	0.0758	0.0018	99.9	1775	3
10207-03G	6.5	571.803	0.019	0.8026	0.0015	0.00960	0.00003	0.0280	0.0007	0.000894	0.000010	0.0682	0.0016	100.0	1813	2
10207-03H	7.0	656.05	0.03	0.9130	0.0015	0.01082	0.00003	0.0298	0.0007	0.000971	0.000010	0.0640	0.0015	100.0	1823.1	1.8
10207-03I	7.5	679.27	0.02	0.9394	0.0016	0.01107	0.00003	0.0271	0.0006	0.001100	0.000010	0.0566	0.0013	100.0	1830.3	1.9
10207-03J	8.0	657.50	0.02	0.9152	0.0015	0.01082	0.00003	0.0233	0.0006	0.001210	0.000011	0.0499	0.0012	99.9	1822.7	1.8
10207-03K	8.5	614.688	0.019	0.8582	0.0015	0.01009	0.00003	0.0217	0.0006	0.001320	0.000012	0.0496	0.0015	99.9	1819	2
10207-03L	9.0	559.367	0.019	0.7873	0.0015	0.00935	0.00002	0.0220	0.0006	0.001520	0.000012	0.0549	0.0015	99.9	1810	2
10207-03M	9.5	465.062	0.017	0.6595	0.0015	0.00800	0.00002	0.0183	0.0006	0.001550	0.000011	0.0545	0.0019	99.9	1801	3
10207-03N	10.0	369.386	0.013	0.5281	0.0014	0.006510	0.000020	0.0149	0.0005	0.001330	0.000010	0.0554	0.0019	99.9	1791	3
10207-03O	10.5	323.229	0.014	0.4638	0.0015	0.00578	0.00002	0.0107	0.0005	0.001050	0.000011	0.045	0.002	99.9	1787	4
10207-03P	11.0	294.768	0.015	0.4180	0.0015	0.005410	0.000020	0.0097	0.0005	0.000936	0.000010	0.046	0.002	99.9	1801	4
10207-03Q	11.5	270.074	0.014	0.3892	0.0016	0.004800	0.000020	0.0156	0.0005	0.000696	0.000009	0.078	0.003	99.9	1782	4
10207-03R	12.0	221.046	0.009	0.3240	0.0016	0.004040	0.000016	0.0135	0.0005	0.000604	0.000009	0.082	0.003	99.9	1763	5
10207-03S	12.5	181.194	0.007	0.2649	0.0016	0.003360	0.000014	0.0105	0.0005	0.000524	0.000008	0.078	0.004	99.9	1766	7
10207-03T	13.0	145.873	0.006	0.2155	0.0015	0.002760	0.000014	0.0089	0.0005	0.000472	0.000007	0.081	0.004	99.9	1754	8
10207-03U	13.5	115.549	0.006	0.1689	0.0015	0.002230	0.000014	0.0066	0.0004	0.000418	0.000008	0.076	0.005	99.9	1766	10
10207-03V	14.0	87.512	0.005	0.1292	0.0015	0.001670	0.000011	0.0052	0.0004	0.000324	0.000007	0.079	0.006	99.9	1755	13
10207-03W	14.5	66.650	0.004	0.0980	0.0015	0.001310	0.000010	0.0042	0.0004	0.000277	0.000007	0.083	0.008	99.9	1759	18
10207-03X	15.0	53.329	0.004	0.0781	0.0016	0.001040	0.000008	0.0037	0.0004	0.000227	0.000006	0.094	0.010	99.9	1764	23
10207-03Y	16.0	44.678	0.005	0.0654	0.0016	0.000904	0.000009	0.0047	0.0005	0.000232	0.000007	0.140	0.014	99.8	1763	28
10207-03Z	18.0	47.210	0.005	0.0736	0.0016	0.000968	0.000008	0.0056	0.0005	0.000241	0.000006	0.150	0.013	99.8	1693	24
10207-03AA	20.0	46.902	0.005	0.0711	0.0015	0.000969	0.000008	0.0053	0.0005	0.000278	0.000007	0.146	0.013	99.8	1724	24
10207-03AB	22.0	34.024	0.004	0.0531	0.0016	0.000734	0.000007	0.0042	0.0004	0.000230	0.000006	0.154	0.016	99.8	1692	33
10207-03AC	24.0	23.236	0.003	0.0359	0.0015	0.000505	0.000006	0.0022	0.0004	0.000181	0.000006	0.12	0.02	99.8	1703	47
10207-03fusior	30.0	25.007	0.004	0.0415	0.0015	0.000673	0.000007	0.0112	0.0006	0.000431	0.000007	0.53	0.03	99.5	1622	39
917A-110R-65-105_mc (J = 0.0023786 ± 0.0000010)																
10210-01A	1.0	0.699	0.002	0.0024	0.0016	0.000298	0.000006	0.0007	0.0004	0.001510	0.000018	0.6	0.5	35.7	410	245
10210-01B	2.0	7.202	0.002	0.0159	0.0016	0.002550	0.000015	0.0023	0.0004	0.01240	0.00005	0.29	0.06	48.6	772	65
10210-01C	2.5	5.615	0.002	0.0218	0.0016	0.001270	0.000011	0.0029	0.0005	0.00529	0.00003	0.26	0.05	71.9	668	40
10210-01D	3.0	6.429	0.002	0.0261	0.0017	0.000934	0.000008	0.0044	0.0005	0.00286	0.00003	0.33	0.04	86.7	752	41
10210-01E	3.5	7.769	0.002	0.0322	0.0016	0.000912	0.000008	0.0057	0.0005	0.00190	0.00002	0.35	0.03	92.7	780	32
10210-01F	4.0	13.559	0.002	0.0418	0.0015	0.001230	0.000010	0.0081	0.0005	0.00240	0.00002	0.38	0.03	94.7	1005	29
10210-01G	4.5	26.384	0.003	0.0624	0.0016	0.001840	0.000011	0.0094	0.0005	0.00429	0.00003	0.295	0.018	95.2	1228	23
10210-01H	5.0	46.784	0.004	0.0790	0.0015	0.002320	0.000012	0.0092	0.0005	0.00597	0.00003	0.227	0.014	96.2	1568	20
10210-01I	5.5	69.786	0.006	0.0991	0.0015	0.002420	0.000014	0.0084	0.0005	0.00604	0.00004	0.166	0.011	97.4	1771	17
10210-01J	6.0	90.104	0.006	0.1150	0.0015	0.002580	0.000014	0.0074	0.0004	0.00597	0.00003	0.127	0.008	98.0	1902	16
10210-01K	6.5	104.130	0.008	0.1273	0.0015	0.002800	0.000014	0.0068	0.0005	0.00631	0.00003	0.105	0.008	98.2	1955	15
10210-01L	7.0	112.539	0.009	0.1382	0.0015	0.002930	0.000016	0.0071	0.0005	0.00612	0.00003	0.101	0.007	98.4	1953	13
10210-01M	7.5	121.409	0.015	0.1535	0.0015	0.003100	0.000014	0.0063	0.0005	0.00600	0.00003	0.080	0.006	98.5	1919	11
10210-01N	8.0	132.258	0.019	0.1666	0.0016	0.003290	0.000016	0.0063	0.0005	0.00594	0.00003	0.074	0.006	98.7	1925	12
10210-01O	8.5	148.233	0.015	0.1851	0.0016	0.003560	0.000018	0.0067	0.0005	0.00573	0.00003	0.071	0.005	98.8	1938	10
10210-01P	9.0	172.34	0.02	0.2107	0.0016	0.003970	0.000016	0.0077	0.0005	0.00556	0.00003	0.072	0.004	99.0	1966	9
10210-01Q	10.0	222.95	0.02	0.2820	0.0016	0.00508	0.00002	0.0086	0.0005	0.00607	0.00003	0.060	0.004	99.2	1926	7
10210-01R	12.0	328.556	0.016	0.4184	0.0016	0.00728	0.00002	0.0121	0.0007	0.00675	0.00004	0.056	0.003	99.4	1921	5
10210-01S	14.0	545.72	0.03	0.6856	0.0016	0.01093	0.00003	0.0172	0.0006	0.00725	0.00004	0.0491	0.0017	99.6	1940	3
10210-01T	16.0	974.06	0.08	1.2112	0.0017	0.01708	0.00004	0.0271	0.0006	0.00877	0.00004	0.0438	0.0011	99.7	1953.5	1.7
10210-01U	16.5	1000.69	0.06	1.2487	0.0017	0.01593	0.00003	0.0404	0.0006	0.00718	0.00004	0.0634	0.0010	99.8	1949.9	1.6
10210-01V	17.0	384.32	0.02	0.5043	0.0017	0.00702	0.00002	0.0403	0.0007	0.00379	0.00003	0.157	0.003	99.7	1889	4
10210-01W	17.5	169.320	0.010	0.2305	0.0016	0.003500	0.000016	0.0364	0.0006	0.00219	0.00002	0.310	0.006	99.6	1845	8
10210-01X	18.0	93.527	0.006	0.1222	0.0015	0.002100	0.000012	0.0309	0.0006	0.001530	0.000018	0.496	0.012	99.5	1892	14
10210-01Y	18.5	60.371	0.005	0.0821	0.0015	0.001440	0.000010	0.0275	0.0006	0.001160	0.000017	0.657	0.019	99.4	1844	21
10210-01Z	19.0	41.074	0.005	0.0558	0.0016	0.001010	0.000009	0.0211	0.0006	0.000868	0.000014	0.74	0.03	99.4	1844	32
10210-01fusior	25.0	34.260	0.003	0.0461	0.0017	0.001010	0.000009	0.0747	0.0010	0.001180	0.000016	3.18	0.12	99.0	1853	44

NOTES:

Samples were irradiated for 9 hours. Sanidine from the Fish Canyon Tuff was used as the neutron fluence monitor with a reference age of 28.201 Ma (Kuiper *et al.*, 2008).

Nucleogenic production ratios:

$(^{36}Ar/^{37}Ar)_{Ca}$ 2.646 ± 0.008 × 1 0^{-4}
$(^{39}Ar/^{37}Ar)_{Ca}$ 6.95 ± 0.09 × 1 0^{-4}
$(^{38}Ar/^{37}Ar)_{Ca}$ 0.196 ± 0.00816
$(^{40}Ar/^{39}Ar)_{K}$ 7.3 ± 0.92 × 1 0^{-4}
$(^{38}Ar/^{39}Ar)_{K}$ 1.22 ± 0.0027 × 1 0^{-2}
$(^{36}Ar/^{38}Ar)_{Cl}$ 3.2 × 1 0^{2}
$^{37}Ar/^{39}Ar$ to Ca/K 1.96

Isotopic constants and decay rates:

$\lambda(^{40}K_{\varepsilon})$ /yr 5.8 ± 0.07 × 1 0^{-11}
$\lambda(^{40}K_{\beta-})$ /yr 4.884 ± 0.0495 × 1 0^{-10}
$\times 10^{-4}$ $\lambda(^{37}Ar)$ /d 1.975 × 1 0^{-2}
$\lambda(^{39}Ar)$ /d 7.068 × 1 0^{-6}
$\lambda(^{36}Cl)$ /d 6.308 × 1 0^{-9}
$(^{40}Ar/^{36}Ar)_{Atm}$ 298.56 ± 0.31
$(^{40}Ar/^{38}Ar)_{Atm}$ 1583.9 ± 2
$^{40}K/K_{Total}$ 0.01167

Tab. 2.

5.2 U-Th/Pb age dating of rock samples from SE Greenland

The U-Th/Pb dating of rock samples from South-East Greenland confirmed the presence of tectono-thermal events in the Archaean and Palaeoproterozoic time as known from the literature and characteristic for the North Atlantic craton and for the Nagssugtoqidian orogen. The data show also the presence of early Mesoproterozoic age events overlapping the timing of the Ammassalik batholith and, finally the presence of Caledonian ages in samples from the Batbjerg area (Fig. 1) at Lat 68ºN as summarized in Figure 2 and the following table.

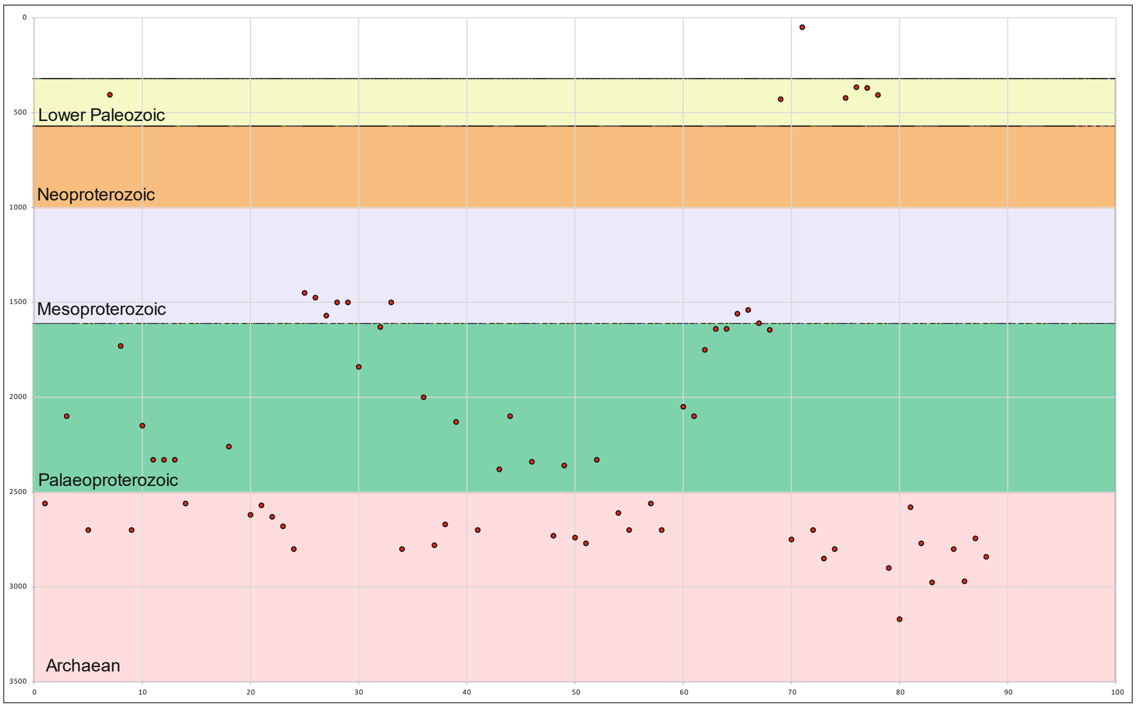

Figure 2. Summary of age distribution of samples analysed in the project.

Sample no.	Sample owner	Minerals dated (no. analyses) zircon (old)	zircon (new)	apatite	monazite	rutile	titanite	U-Th-Pb Geochronology results (see attached plots)
288112	GEUS	zir			mon (6)	rut (53)		**Rutile** intercept age (Wetherill, anchored at 0 Ma) at 2563 Ma +/-12; Intercept age for TW (2285 Ma!) not reliable **Monazite:** few monazite grains! Monazite upper intercept (large uncertaincy): Wetherill = 2991 +/-745 Ma; TW = 3127 +/-439 Ma; Lower intercept not reliable due to too large uncertaincies.
288112	GEUS	zir						
288143	GEUS	zir		apa (49)				**Apatite** lower intercept: Wetherill = 2100 +/-36 Ma; TW = 2112 +/-26 Ma
288143	GEUS	zir						
288145	GEUS	zir		apa (4)	mon (17)			**Monazite** upper intercept age for 2 of the grains: Wetherill = 2734 +/- 74 Ma; TW = 2769 +/-21 Ma; **Apatite**: No trend could be determined, but most probably very old (Achean);
288145	GEUS	zir						
312981	GEUS	zir				rut (20)		**Rutile** lower intercept age: Wetherill = 406 Ma +/-13; TW = 412 Ma +/-12; Rutile median 206/238 Pbc-age = 410 +/-31 Ma
473710	GEUS	?				rut (42)		**Rutile** intercept age: Wetherill (anchored at 0 Ma) = 1732 Ma +/-20; TW = 1778 Ma +/-? (not reliable!); Rutile median 7/6age at 1722 +/-26 Ma
509319	GEUS	zir			mon (5) mon (38)			**1. run**: (5 grains only): **Monazite** upper intercept age: Wetherill = 2699 +/- 8 Ma; TW = 2703 +/-3 Ma **2. run** (38 grains): Wetherill = 2699 +/- 8 Ma; TW = 2781 +/-19 Ma
509328	GEUS	zir		apa (20)				**Apatite** lower intercept: Wetherill = 2151 +/-79 Ma, TW= 2136 +/-58 Ma
509345	GEUS	zir		apa (22)				**Apatite** lower intercept: Wetherill = 2332 +/-71 Ma; TW = 2348 +/-51 Ma
509345	GEUS	zir						
516105	GEUS	zir		apa (13)				**Apatite** lower intercept: Wetherill = 2328 +/-50 Ma, TW= 2335 +/-35 Ma
516106	GEUS	zir				rut (91)		**Rutile** intercept age: Wetherill (anchored at 0 Ma) = 2567 Ma +/-10; TW = 2653 Ma +/-5 (not reliable!); Rutile median 7/6age at 2566 +/-6 Ma
516106	GEUS	zir						
516106	GEUS	zir						
516106	GEUS	zir						
516117	GEUS	zir		apa (20)				**Apatite** lower intercept: Wetherill = 2262 +/-118 Ma; TW = 2289 +/-86 Ma
516117	GEUS	zir						
516151	GEUS	zir			mon (3)			**Monazite:** only 3 grains! Monazite upper intercept age: Wetherill = 2626 +/- ? Ma; TW = 2656 +/-49 Ma; Monazite lower intercept age (very uncertain!): Wetherill = 1852 +/-?Ma, TW = 1737 +/-537 Ma
516157	GEUS	zir					tit (34)	**Titanite** upper intercept (anchored at 0 Ma): Wetherill = 2618 +/-36 Ma (Pbc); TW = 2604 +/-19 Ma (Pbc); Titanite Concordia age: Wetherill = 2582 +/-10 Ma; TW = 2570 +/-7 Ma
516163	GEUS	zir			mon (3)			**Monazite:** only 3 grains! Monazite upper intercept age for 2 of the grains: Wetherill = 2628 +/- ? Ma
516171	GEUS	zir					tit (94)	**Titanite** upper intercept: Wetherill = 2680 +/-36 Ma (Pbc); TW = 2680+/- 25 Ma (Pbc); Titanite lower intercept not reliable; Titanite median 7/6 Pbc-age (3 S.D. rejection) at 2664 +/-9 Ma
523927	GEUS	zir			mon (61)			**Monazite** upper intercept age: Wetherill = 2799 +/- 41 Ma; TW = 2778 +/- 15 Ma; Monazite lower intercept age (very uncertain!): Wetherill = 922 +/- 370 Ma, TW = 906 +/-155 Ma
525203	GEUS	zir		apa (59)			tit (72)	**Apatite** lower intercept: Wetherill = 1445 +/-16 Ma, TW= 1454 +/-12 Ma; **Titanite** upper intercept (anchored at 0 Ma): Wetherill = 1653 +/-19 Ma (Pbc); TW = 1610 +/-7 Ma (Pbc); Titanite Concordia age: Wetherill = 1579 +/-3 Ma; TW = 1573 +/-3 Ma
525204	GEUS	zir		apa (55)			tit (91)	**Apatite** lower intercept: Wetherill = 1475 +/-38 Ma, TW= 1498 +/-28 Ma; **Titanite** lower intercept: Wetherill = 1472 +/-12 Ma or 1465 +/-15 Ma (Pbc); TW = 1480 +/-9 Ma or 1474 +/-8 Ma (Pbc)
525205	GEUS	zir		apa(46)			tit (54)	**Apatite** lower intercept: Wetherill = 1386 +/-18 Ma, TW= 1408 +/-13 Ma; **Titanite** intercept (anchored at 0 Ma): Wetherill = 1571 +/-10 Ma (Pbc); TW = 1616 +/-28 Ma (Pbc); Titanite Concordia age unlikely
525206	GEUS	zir		apa(78)			tit (64)	**Apatite** lower intercept: Wetherill = 1476 +/-10 Ma, TW= 1481 +/-8 Ma; **Titanite** lower intercept (anchored at 0 Ma): Wetherill = 1507 +/-32 Ma (Pbc); TW = 1507 +/-17 Ma (Pbc); Titanite upper intercept not reliable; Titanite Concordia age: Wetherill = 1536 +/-4 Ma; TW = 1530 +/-3 Ma
525231	GEUS	?		apa(91)				**Apatite** lower intercept: Wetherill = 1496 +/-5 Ma, TW= 1499 +/-3 Ma;
525233	GEUS	zir		apa(74)			tit (70)	**Apatite** lower intercept: Wetherill = 1451 +/-9 Ma, TW= 1451 +/-6 Ma; **Titanite** upper intercept (anchored at 0 Ma): Wetherill = 1843 +/-8 Ma (Pbc); TW = 1769 +/-3 Ma (Pbc); Titanite Concordia age unlikely
525233	GEUS	zir						
525258	GEUS	zir					tit (52)	**Titanite** upper intercept (anchored at 0 Ma): Wetherill = 1625 +/-11 Ma (Pbc); TW = 1591 +/-5 Ma (Pbc); Titanite median 7/6 Pbc-age (3 S.D. rejection) = 1630 +/-7 Ma; Concordia age unlikely

525260	GEUS	zir		apa (32)	mon (69)		tit (62)	Apatite lower intercept: Wetherill = 1495 +/-28 Ma; TW = 1506 +/-22 Ma; **Probably detrital titanites**. Titanite age spread from 1500 to 1850 Ma with inherited age at 2340+2435 Ma; ***Probably detrital monazites (no Pbc)***. One concordant monazite age at 1776 Ma (OK!); For the rest: Monazite upper intercept age (uncertain!): Wetherill = 2134 +/-85 Ma; TW = 2720 +/-130 Ma2000 Ma; Monazite lower intercept
527010	GEUS	zir			mon (89)			**Probably detrital monazites** due to large relatively spread. Monazite upper intercept: Wetherill = 2797 +/-5 Ma (anchored at 0 Ma); TW = incorrect intercept
527010	GEUS	zir						
527435	GEUS	zir		apa (51)				**Apatite** lower intercept: Wetherill = 1990 +/-58 Ma; TW = 2001 +/-42 Ma
527454	GEUS	zir			mon (23)			**Monazite** upper intercept age: Wetherill = 2784 +/- 74 Ma; TW = 2763 +/- 21 Ma; Monazite lower intercept age useless
527505	GEUS	zir			mon (24)			**Monazite** upper intercept: Wetherill = 2669 +/-46 Ma; TW = 2684 +/-23 Ma
527528	GEUS	zir		apa (51)				**Apatite** lower intercept: Wetherill = 2137 +/-106 Ma; TW = 2167 +/-29 Ma
527528	GEUS	zir						
527557	GEUS	zir			mon (15)			**Monazite** upper intercept age: Wetherill = 2698 +/- 36 Ma; TW = 2710 +/- 18 Ma; Monazite lower intercept age useless
527557	GEUS	zir						
527609	GEUS	zir		apa (86)				**Apatite** lower intercept: Wetherill = 2386 +/-66 Ma or 2403 +/-9 Ma (Pbc); TW = 2392 +/-52 Ma or 2409 +/-16 Ma (Pbc)
527650	GEUS	zir		apa (20)				**Apatite** lower intercept: Wetherill = 2030 +/-267 Ma; TW = 2106 +/-164 Ma
527650	GEUS	zir						
527678	GEUS	zir		apa (41)				**Apatite** lower intercept: Wetherill = 2340 +/-89 Ma; TW = 2363 +/-61 Ma
527678	GEUS	zir						
528621	GEUS	zir					tit (3)	**Titanite** upper intercept (3 grains only!): Wetherill = 2732 +/-? Ma; TW = 2750 +/-1 Ma; ; Titanite Concordia age: Wetherill = 2738 +/-9 Ma; TW = ConAge unlikely
528641	GEUS	zir					tit (104)	**Titanite** lower intercept: Wetherill = 2364 +/-85 Ma and 2280 +/-208 Ma (Pbc); TW = 2457 +/-51 Ma and 2314 +/-132 Ma (Pbc); Titanite upper intercept not reliable; Titanite Concordia age = 2581 +/-8 Ma (but discordant)
528651	GEUS	zir		apa (29)			tit (35)	**Apatite** lower intercept: Wetherill = 2742 +/-10 Ma; TW = 2752 +/-2 Ma; Apatite median 7/6 age (3 S.D. rejection) at 2751 +/-8 Ma; **Titanite** upper intercept (Pbc): Wetherill = 2750 +/-109 Ma; TW = 2790 +/- 110 Ma
535905	GEUS	zir			mon (65)			**Monazite** upper intercept: Wetherill = 2775 +/-16 Ma, TW = and 2773 +/-7 Ma; Monazite lower intercept: Wetherill = 708 +/282 Ma, TW = and 732 +/-112 Ma (NB: large uncertaincy!);
535925	GEUS	zir		apa (91)				**Apatite** lower intercept: Wetherill = 2229 +/-36 Ma; TW = 2243 +/-26 Ma
535925	GEUS	zir						
535962	GEUS	zir			mon (57)			Probably two **monazite** age populations at ca. 2610 Ma (concordant) and a discordant at ca. 2100-2200 Ma (discordant, lower intercept) whatever this age means(?). Alternatively, detrital monazites due to spread.
536517	GEUS	zir		apa (23)		-		**Apatite** lower intercept: Wetherill = 1588 +/-80 Ma, TW = 1595 +/-47 Ma; Apatite upper intercept: Wetherill = 2698 +/-88 Ma, TW = 2726 +/-24 Ma;
536517	GEUS	zir						
536588	GEUS	zir				rut (41)		**Rutile** lower intercept: Wetherill (anchor at 0 Ma) = 2560 Ma +/-18; Intercept age for TW (2285 Ma!) not reliable; Median 7/6-age = 2565 +/- 12 Ma.
542032	GEUS	zir					tit (26)	**Titanite** upper intercept: Wetherill = 2729 +/-146 Ma and 2686 +/-104 Ma (Pbc); TW = not reliable and 2777+/-145 Ma (Pbc); Titanite lower intercept not reliable; Titanite median 7/6 Pbc-age (3 S.D. rejection) at 2670 +/-5 Ma
542032	GEUS	zir						
542059	GEUS	zir		apa (10)				**Apatite** lower intercept: Wetherill = 2047 +/-54 Ma; TW = 2044 +/-34 Ma
542074	GEUS	zir		apa (11)				**Apatite** lower intercept: Wetherill = 2111 +/-209 Ma; TW = 2182 +/-137 Ma NB: (large uncertaincy!)
562814	GEUS	zir			mon (81)			Two **Monazite** age populations: **(1)** Monazite upper intercept: Wetherill = 1799 +/-25 Ma, TW = and 1750 +/-10 Ma (uncertain intercept!); **(2)** Monazite upper intercept: Wetherill = 2025 +/-96 Ma, TW = and 2064 +/- 47 Ma; Monazite lower intercept: **(1)** Wetherill = 761 +/318 Ma, TW = and 895 +/-114 Ma (NB: large uncertaincy!); **(2)** no intercept;
562901	GEUS	zir					tit (83)	**Titanite** upper intercept: Wetherill = 1642 +/-30 Ma (Pbc); TW = 1609 +/- 13 Ma (Pbc); Titanite lower intercept not reliable; Titanite median 7/6 Pbc-age (3 S.D. rejection) = 1654 +/-7 Ma
562910	GEUS	zir		apa (26)			tit (66)	**Apatite** lower intercept: Wetherill = 1418 +/-44 Ma; TW = 1432 +/-33 Ma; **Titanite** upper intercept: Wetherill = 1641 +/-24 Ma (Pbc); TW = 1588 +/-9 Ma (Pbc); Titanite median 7/6 Pbc-age (3 S.D. rejection) = 1634 +/-18 Ma; Titanite Concordia age (Wetherill, Pbc): 1560 +/-6 Ma
562921	GEUS	zir		apa (91)				**Apatite** lower intercept (Wetherill) at 1561 +/-20 Ma; Apatite lower intercept (TW) at 1560 +/-14 Ma

562936	GEUS	zir		apa (1)			tit (6)	**Titanite** intercept (6 grains only!): Wetherill (anchored at 0 Ma) = 1464 +/-97 Ma; TW (anchored at 0 Ma) = 1542 +/-34 Ma; TW (un-anchored) = 1547 +/-48 Ma; **Apatite:** 1 very discordant grains = not reliable age
563965	GEUS	zir		apa (3)			tit (80)	**Apatite** lower intercept: Wetherill = 1613 +/-136 Ma, TW= 1690 +/-126 Ma (3 analyses = large uncertainty!); **Titanite** lower intercept: Wetherill = 1408 +/-56 Ma or 1430 +/-45 Ma (Pbc); TW = 1523 +/-2 Ma or 1474 +/-11 Ma (Pbc)
564634	GEUS	zir					tit (70)	**Titanite** upper intercept (anchored at 0 Ma): Wetherill = 1645 +/-17 Ma (Pbc); TW = 1617 +/-7 Ma (Pbc); Titanite median 7/6 Pbc-age (3 S.D. rejection) = 1624 +/-19 Ma
3206/7A	KU		zir (83)	apa (51)			tit (90)	**Zircon** of Caledonian ages with lower intercepts at 429 +/-1 Ma (no PbC correction) with age variation from ca. 380/400 Ma to 500 Ma. **Titanite** lower intercept: TW = 408 +/-6 Ma; Titanite upper intercept not reliable; **Apatite** lower intercept: Wetherill = 385 +/-24 Ma; TW = 378 +/-10 Ma;
27842B	KU		zir (31)	apa (26)				**Zircon** 207/206 ages from 2713 to 2755 Ma. Upper intercept at 2758 +/-4 Ma. **Apatite:** Scattered and no distinct age trends (maybe young?);
27846	KU		zir (124)	apa (48)				**Zircon** upper intercept at 3056 +/-5 Ma. Lower intercept at 178 +/-24 Ma (uncertain); **Apatite** lower intercept: Wetherill = 41 +/-15 Ma; TW = 63 +/-9 Ma;
27851	KU		zir (127)	apa (24)				**Zircon** upper intercept at 2719 +/-5 Ma. Lower intercept bad. **Apatite:** scattered but most probably Proterozoic ages at round 1400-2200 Ma (best guess so not really reliable)
27863	KU		zir (124)	apa (2)				**Zircon:** Two major zircon populations with upper intercept at ca. 2850-2870 Ma and at ca. 3180 Ma, respectively. Lower intercept might be at around 400-450 Ma (uncertain). **Apatite**: Two single grains both with ages at 2850 Ma
27865	KU		zir (100)					**Zircon:** One or two major zircon populations with upper intercept at ca. 2800 Ma and at 2850 Ma, respectively. No ages below 2600 Ma
30201	KU			apa ()			tit (8)	**Titanite** lower intercept: TW = 423 +/-12 Ma (8 analyses only!); Titanite upper intercept not reliable; **Apatite** lower intercept: Wetherill = 391 +/-20 Ma; TW = 391 +/-9 Ma;
30203	KU			apa (8)				**Apatite** lower intercept: Wetherill = 366 +/-?? Ma; TW = 303 +/-235 Ma (very uncertain)
30231	KU			apa (84)		rut (32)		**Apatite** lower intercept: Wetherill = 370 +/-9 Ma; TW = 370 +/-32 Ma; **Rutile** lower intercept: Wetherill = 460+/-4 Ma; TW = 467+/-10 Ma;
30242	KU			apa (32)			tit (83)	**Titanite** lower intercept: TW = 407 +/-7 Ma; Titanite upper intercept not reliable. **Apatite** lower intercept: Wetherill = 370 +/-14 Ma; TW = 395 +/-9 Ma;
30271	KU		zir (10)					**Zircon** analyses all above Concordia, so less reliable. Nevertheless, all ages are >2900 Ma (youngest recorded).
30275	KU		zir (53)	apa (74)				**Zircon** upper intercept at 3172 +/-4 Ma (Pbc + no-Pbc). Lower intercept too uncertain (736 Ma). **Apatite** lower intercept: Wetherill = 361 +/-5 Ma; TW = 362 +/-3 Ma;
27837A	KU		zir (81)					**Zircon** upper intercept at 2582 +/-13 Ma. Lower intercept at 99 +/-3 Ma. Data very discordant and all data Pbc-corrected, thus intercept ages somewhat uncertain!!
27840B	KU		zir (116)	apa (2)	mon (7)			**Zircon:** Two major zircon populations with upper intercept at ca. 2770-2850 Ma and at 3000, respectively. **Monazite** upper intercept age (7 analyses): Wetherill = 2739 +/- 65 Ma; **Apatite**: Two grains with one "decent" age at ca. 3321+/-23 Ma (discordant and can probably not be trusted!)
27843B	KU		zir (44)	apa (3)				**Zircon** upper intercept at 2976 +/-32 Ma. Lower intercept at 173 +/-22 Ma (uncertain). Data very discordant!! **Apatite:** present, but no age calculation could be estimated
27847A	KU	-	-	-	-	-	-	-
27848A	KU		zir (108)	apa (53)	mon (19)			**Zircon:** Two major zircon populations with upper intercept at ca. 2800 Ma and at 3000 Ma, respectively. **Monazite** upper intercept: Wetherill (anchored) = 2748 +/-9 Ma; **Apatite:** scattered (no distinct age trend)
27854C	KU		zir (91)	apa (38)				**Zircon:** Two major zircon populations with upper intercept at ca. 2970-2980 Ma and at 3140 +/-5 Ma, respectively. The old population has an uncertain lower intercept at 395 +/-37 Ma. **Apatite:** Scattered and no distinct trend. However, probably more populations with one possible lower intercept (4 grains) of ca. 450 Ma. Most analyses are older with most probably Proterozoic or Archean ages;
27860BI	KU		zir (67)	apa (16)	mon (72)			**Zircon** upper intercept at 2744 +/-11 Ma and an (uncertain) lower intercept at 83 +/-9 Ma. **Monazite** upper intercept: Wetherill = 2792 +/-41 Ma; **Apatite**: scattered (no robust age could be calculated)
27864D	KU		zir (110)	apa (0)	mon (70)			**Zircon** upper intercept at 2841 +/-1 Ma and an uncertain lower intercept at 436 +/- 103 Ma. **Monazite** upper intercept: Wetherill = 2718 +/-22 Ma. **Apatite** present, but no age calculations possible;

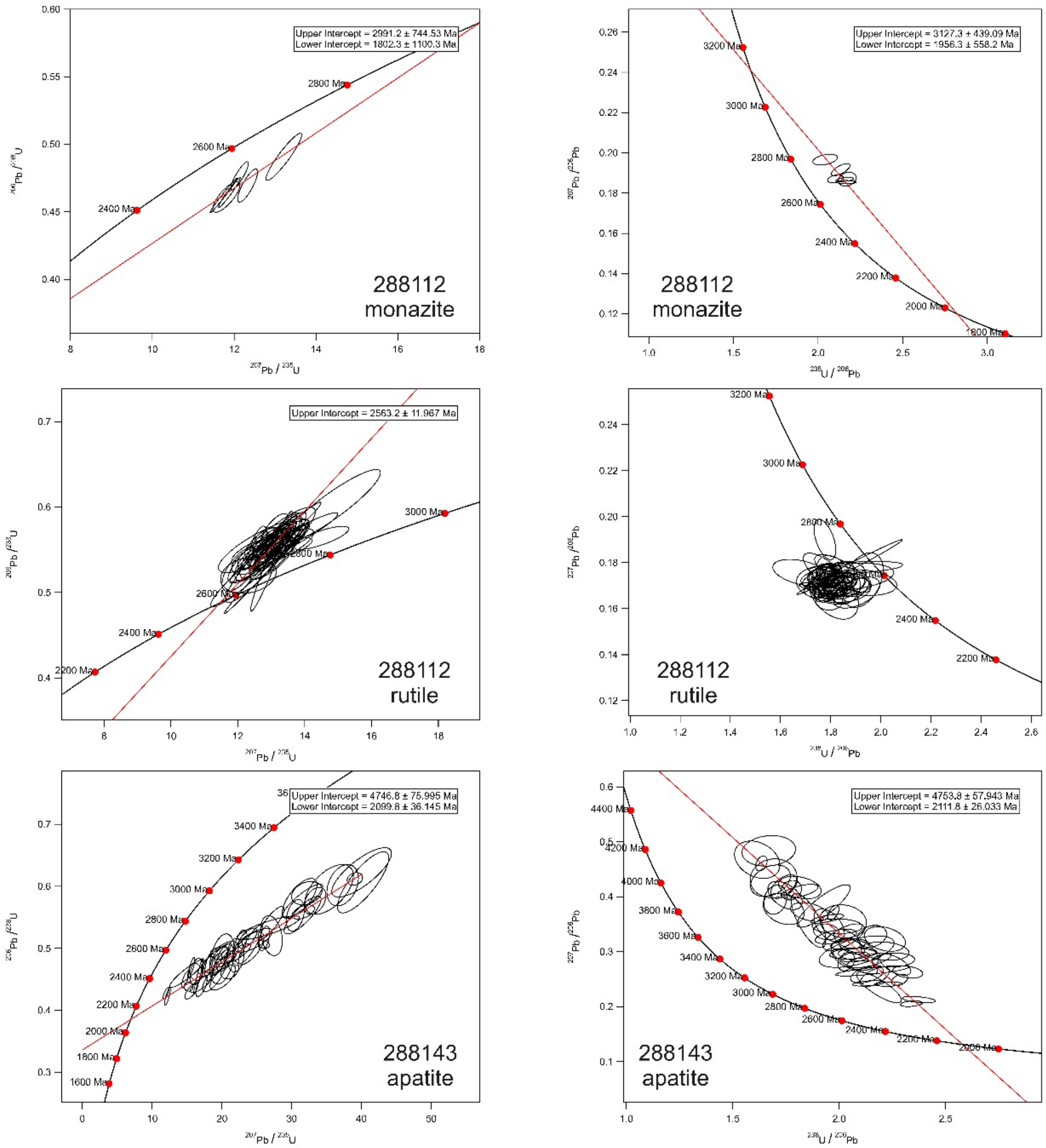
Upper Intercept = 2991.2 ± 744.53 Ma
Lower Intercept = 1802.3 ± 1100.3 Ma
288112
monazite
Upper Intercept = 3127.3 ± 439.09 Ma
Lower Intercept = 1956.3 ± 558.2 Ma
288112
monazite
Upper Intercept = 2563.2 ± 11.967 Ma
288112
rutile
288112
rutile
Upper Intercept = 4746.8 ± 75.995 Ma
Lower Intercept = 2099.8 ± 36.145 Ma
288143
apatite
Upper Intercept = 4753.8 ± 57.943 Ma
Lower Intercept = 2111.8 ± 26.033 Ma
288143
apatite

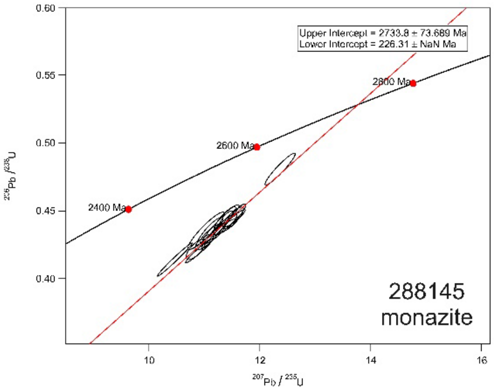
Upper Intercept = 2733.8 ± 73.689 Ma
Lower Intercept = 226.31 ± NaN Ma
288145
monazite

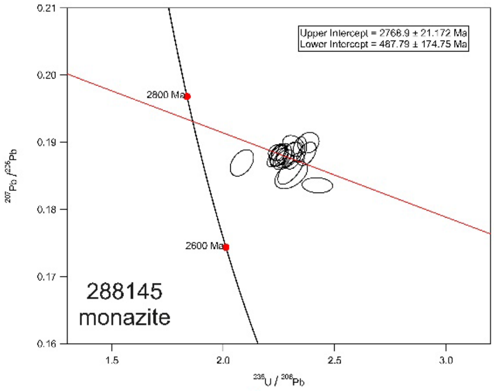
Upper Intercept = 2768.9 ± 21.172 Ma
Lower Intercept = 487.79 ± 174.75 Ma
288145
monazite

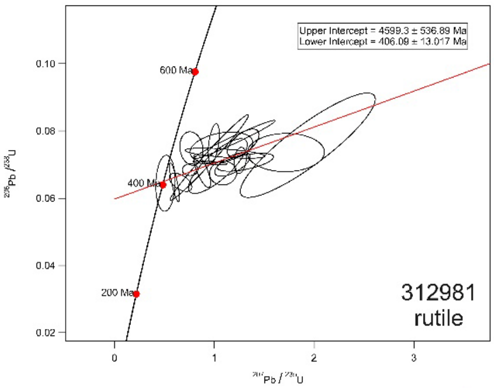
Upper Intercept = 4599.3 ± 536.89 Ma
Lower Intercept = 406.09 ± 13.017 Ma
312981
rutile

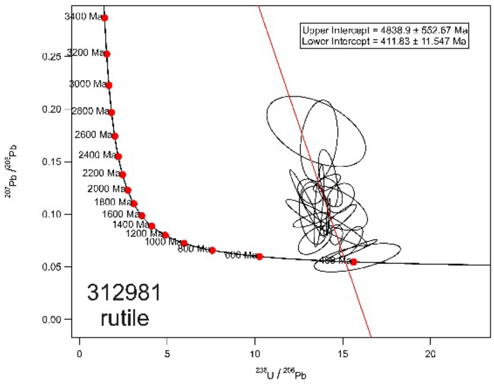
Upper Intercept = 4838.9 ± 552.67 Ma
Lower Intercept = 411.83 ± 11.547 Ma
312981
rutile

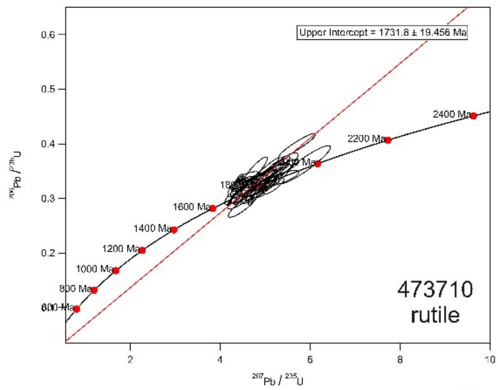
Upper Intercept = 1731.8 ± 19.456 Ma
473710
rutile

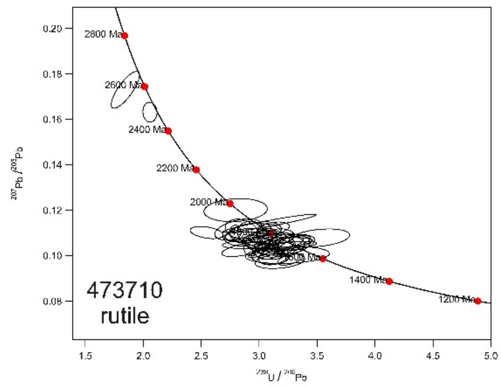
473710
rutile

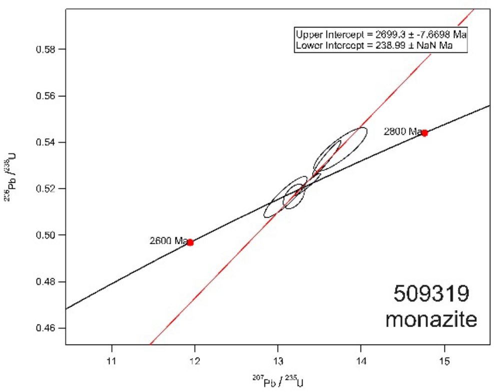
Upper Intercept = 2699.3 ± -7.6698 Ma
Lower Intercept = 238.99 ± NaN Ma
509319
monazite

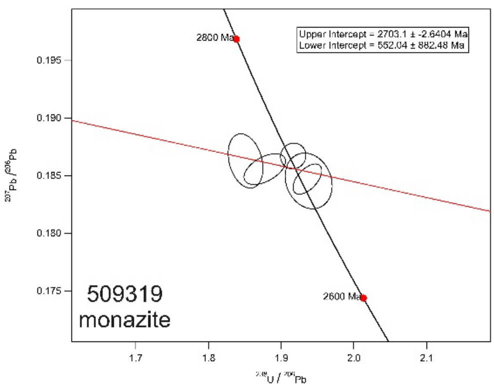
Upper Intercept = 2703.1 ± -2.6404 Ma
Lower Intercept = 552.04 ± 882.48 Ma
509319
monazite

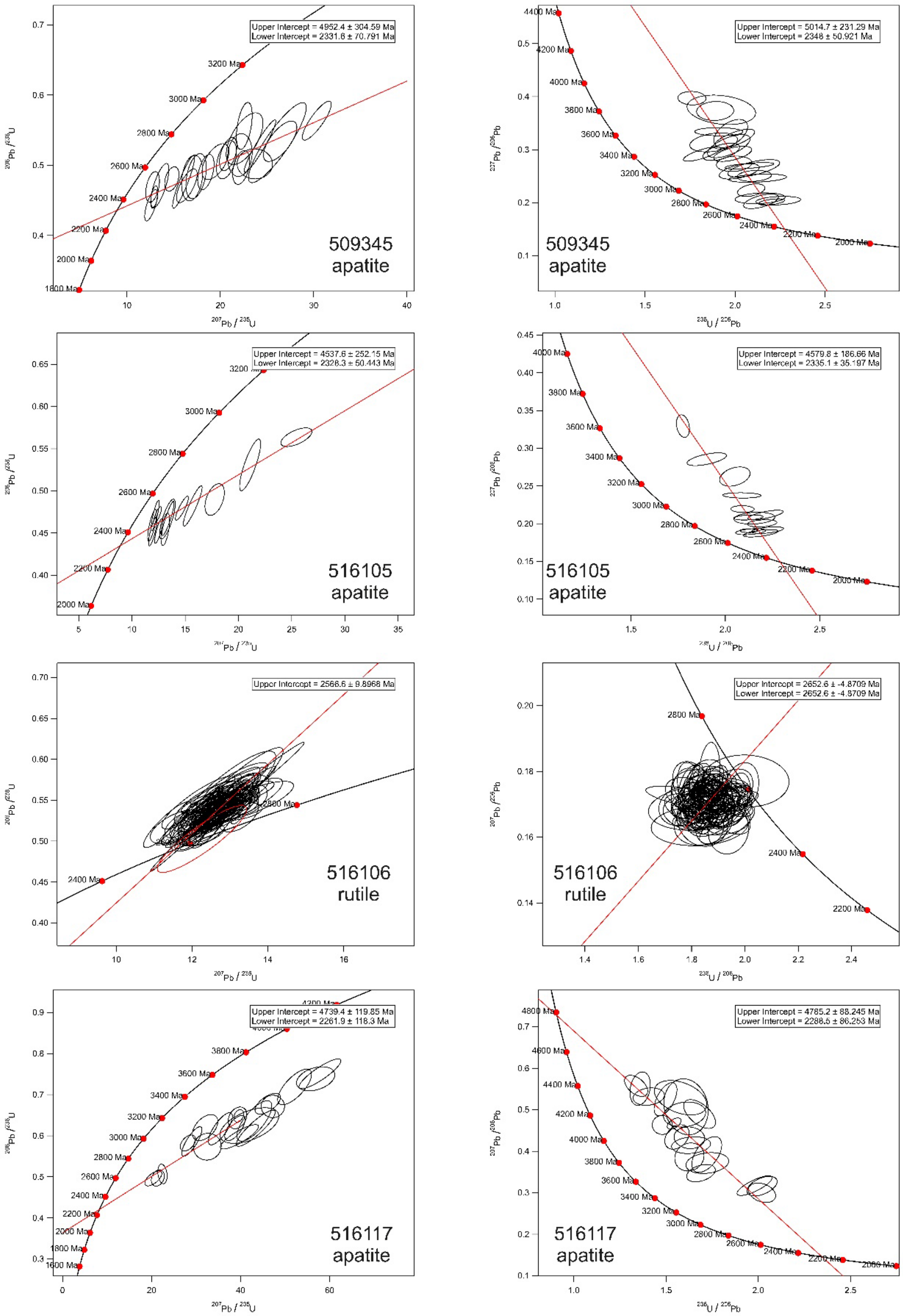
Upper Intercept = 4952.4 ± 304.59 Ma
Lower Intercept = 2331.6 ± 70.791 Ma
509345
apatite
Upper Intercept = 5014.7 ± 231.29 Ma
Lower Intercept = 2348 ± 50.921 Ma
509345
apatite
Upper Intercept = 4537.6 ± 252.15 Ma
Lower Intercept = 2328.3 ± 50.443 Ma
516105
apatite
Upper Intercept = 4579.8 ± 186.66 Ma
Lower Intercept = 2335.1 ± 35.197 Ma
516105
apatite
Upper Intercept = 2566.6 ± 9.8968 Ma
516106
rutile
Upper Intercept = 2652.6 ± -4.8709 Ma
Lower Intercept = 2652.6 ± -4.8709 Ma
516106
rutile
Upper Intercept = 4739.4 ± 119.85 Ma
Lower Intercept = 2261.9 ± 118.3 Ma
516117
apatite
Upper Intercept = 4785.2 ± 88.245 Ma
Lower Intercept = 2288.5 ± 86.253 Ma
516117
apatite

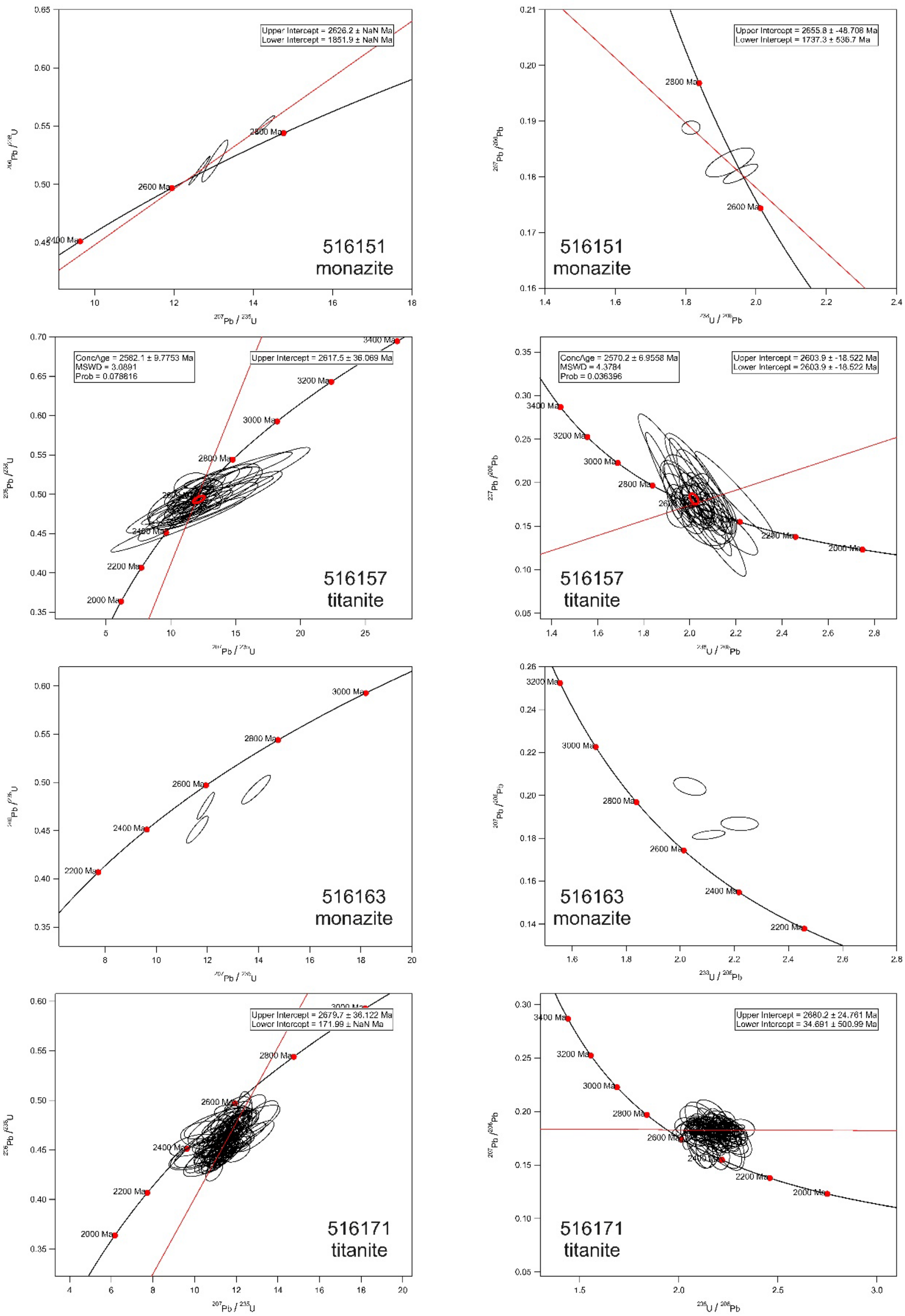
Upper Intercept = 2626.2 ± NaN Ma
Lower Intercept = 1851.9 ± NaN Ma
516151
monazite
Upper Intercept = 2655.8 ± -48.708 Ma
Lower Intercept = 1737.3 ± 536.7 Ma
516151
monazite
ConcAge = 2582.1 ± 9.7753 Ma
MSWD = 3.0891
Prob = 0.078816
Upper Intercept = 2617.5 ± 36.069 Ma
516157
titanite
ConcAge = 2570.2 ± 6.9558 Ma
MSWD = 4.3784
Prob = 0.036396
Upper Intercept = 2603.9 ± -18.522 Ma
Lower Intercept = 2603.9 ± -18.522 Ma
516157
titanite
516163
monazite
516163
monazite
Upper Intercept = 2679.7 ± 36.122 Ma
Lower Intercept = 171.99 ± NaN Ma
516171
titanite
Upper Intercept = 2680.2 ± 24.761 Ma
Lower Intercept = 34.691 ± 500.99 Ma
516171
titanite

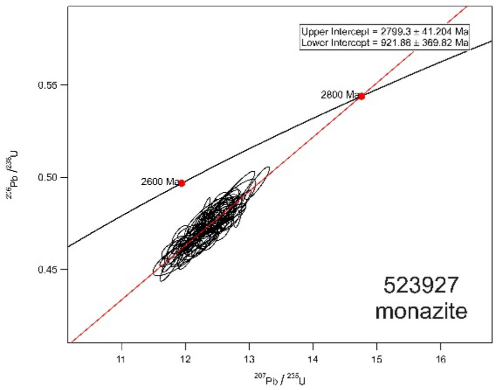
Upper Intercept = 2799.3 ± 41.204 Ma
Lower Intercept = 921.88 ± 369.82 Ma
2800 Ma
2600 Ma
523927
monazite
$^{207}Pb / ^{235}U$
$^{206}Pb / ^{238}U$

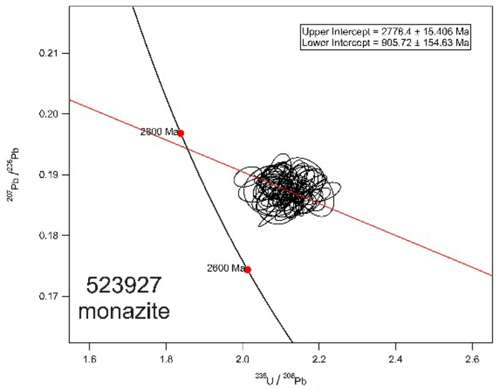
Upper Intercept = 2776.4 ± 15.406 Ma
Lower Intercept = 905.72 ± 154.63 Ma
2800 Ma
2600 Ma
523927
monazite
$^{238}U / ^{206}Pb$
$^{207}Pb / ^{206}Pb$

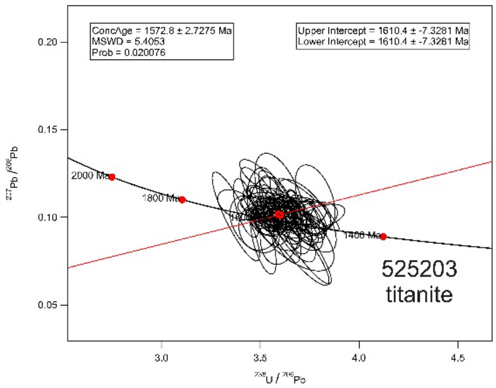
ConcAge = 1572.8 ± 2.7275 Ma
MSWD = 5.4053
Prob = 0.020076
Upper Intercept = 1610.4 ± -7.3281 Ma
Lower Intercept = 1610.4 ± -7.3281 Ma
2000 Ma
1800 Ma
1400 Ma
525203
titanite
$^{238}U / ^{206}Pb$
$^{207}Pb / ^{206}Pb$

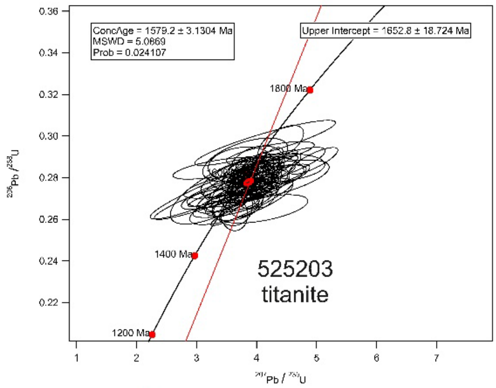
ConcAge = 1579.2 ± 3.1304 Ma
MSWD = 5.0669
Prob = 0.024107
Upper Intercept = 1652.8 ± 18.724 Ma
1800 Ma
1400 Ma
1200 Ma
525203
titanite
$^{207}Pb / ^{235}U$
$^{206}Pb / ^{238}U$

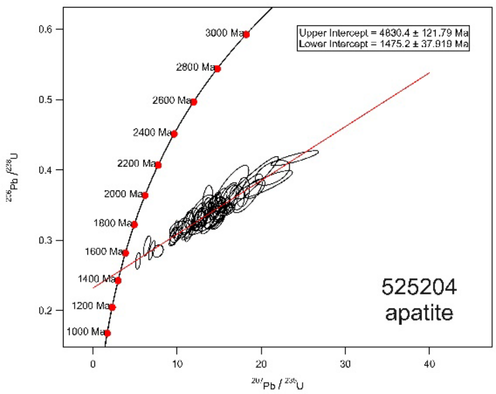
Upper Intercept = 4830.4 ± 121.79 Ma
Lower Intercept = 1475.2 ± 37.919 Ma
3000 Ma
2800 Ma
2600 Ma
2400 Ma
2200 Ma
2000 Ma
1800 Ma
1600 Ma
1400 Ma
1200 Ma
1000 Ma
525204
apatite
$^{207}Pb / ^{235}U$
$^{206}Pb / ^{238}U$

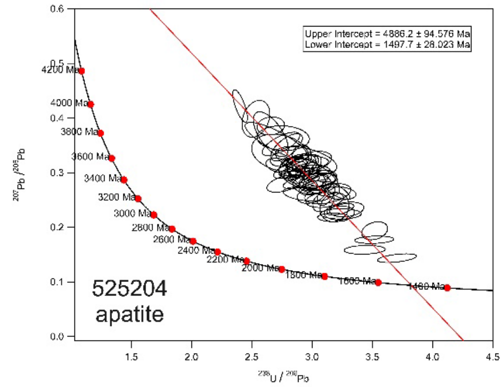
Upper Intercept = 4886.2 ± 94.576 Ma
Lower Intercept = 1497.7 ± 28.023 Ma
4200 Ma
4000 Ma
3800 Ma
3600 Ma
3400 Ma
3200 Ma
3000 Ma
2800 Ma
2600 Ma
2400 Ma
2200 Ma
2000 Ma
1800 Ma
1600 Ma
1400 Ma
525204
apatite
$^{238}U / ^{206}Pb$
$^{207}Pb / ^{206}Pb$

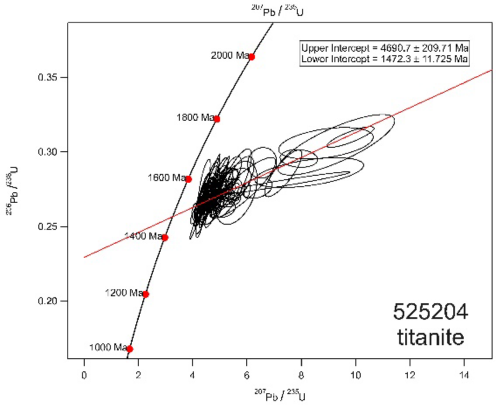
Upper Intercept = 4690.7 ± 209.71 Ma
Lower Intercept = 1472.3 ± 11.725 Ma
2000 Ma
1800 Ma
1600 Ma
1400 Ma
1200 Ma
1000 Ma
525204
titanite
$^{207}Pb / ^{235}U$
$^{206}Pb / ^{238}U$

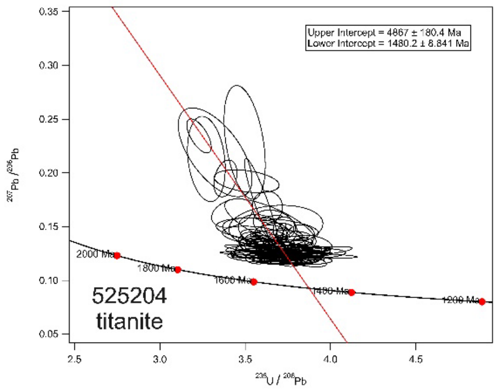
Upper Intercept = 4867 ± 180.4 Ma
Lower Intercept = 1480.2 ± 8.841 Ma
2000 Ma
1800 Ma
1600 Ma
1400 Ma
1200 Ma
525204
titanite
$^{238}U / ^{206}Pb$
$^{207}Pb / ^{206}Pb$

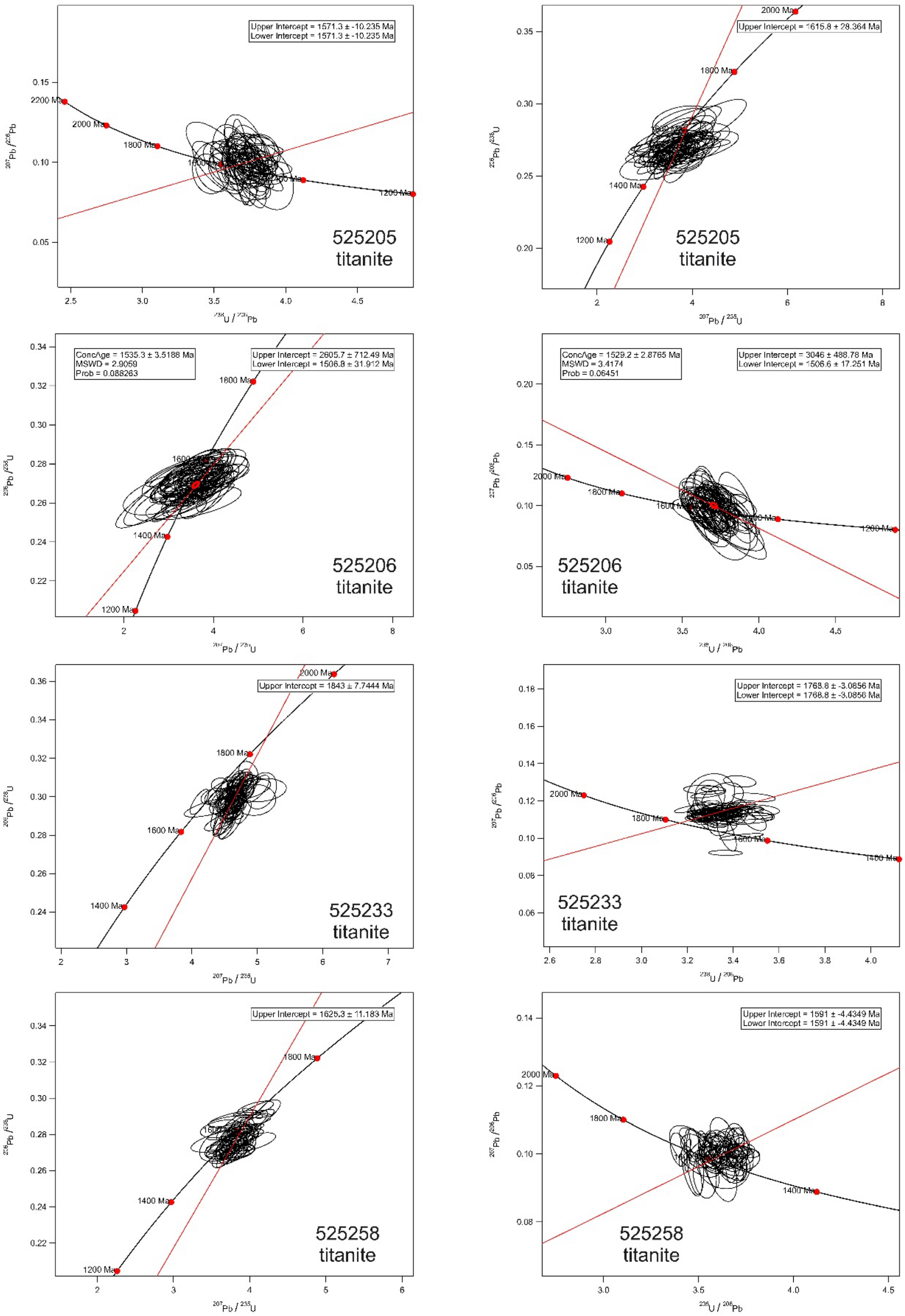
Upper Intercept = 1571.3 ± -10.235 Ma
Lower Intercept = 1571.3 ± -10.235 Ma
2200 Ma
2000 Ma
1800 Ma
1200 Ma
525205
titanite
Upper Intercept = 1615.8 ± 28.364 Ma
2000 Ma
1800 Ma
1400 Ma
1200 Ma
525205
titanite
ConcAge = 1535.3 ± 3.5188 Ma
MSWD = 2.9059
Prob = 0.088263
Upper Intercept = 2605.7 ± 712.49 Ma
Lower Intercept = 1506.8 ± 31.912 Ma
1800 Ma
1400 Ma
1200 Ma
525206
titanite
ConcAge = 1529.2 ± 2.8765 Ma
MSWD = 3.4174
Prob = 0.06451
Upper Intercept = 3046 ± 488.78 Ma
Lower Intercept = 1506.6 ± 17.251 Ma
2000 Ma
1800 Ma
1200 Ma
525206
titanite
Upper Intercept = 1843 ± 7.7444 Ma
2000 Ma
1800 Ma
1600 Ma
1400 Ma
525233
titanite
Upper Intercept = 1768.8 ± -3.0856 Ma
Lower Intercept = 1768.8 ± -3.0856 Ma
2000 Ma
1800 Ma
1400 Ma
525233
titanite
Upper Intercept = 1625.3 ± 11.183 Ma
1800 Ma
1400 Ma
1200 Ma
525258
titanite
Upper Intercept = 1591 ± -4.4349 Ma
Lower Intercept = 1591 ± -4.4349 Ma
2000 Ma
1800 Ma
1400 Ma
525258
titanite

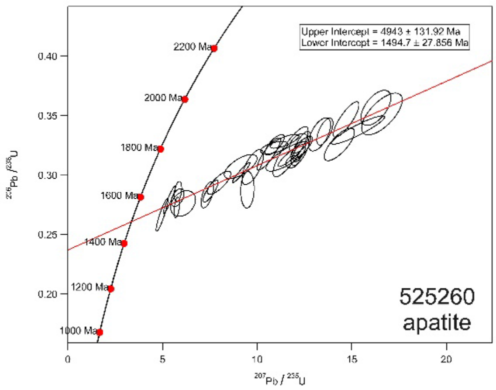
Upper Intercept = 4943 ± 131.92 Ma
Lower Intercept = 1494.7 ± 27.856 Ma
525260
apatite

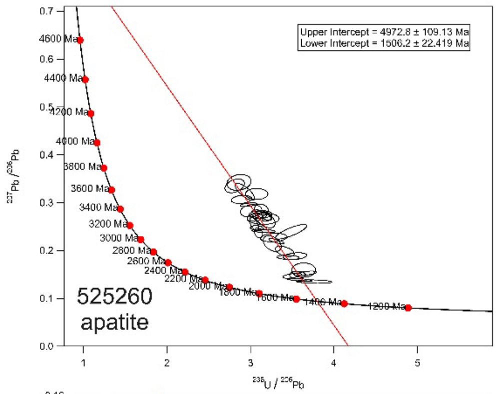
Upper Intercept = 4972.8 ± 109.13 Ma
Lower Intercept = 1506.2 ± 22.419 Ma
525260
apatite

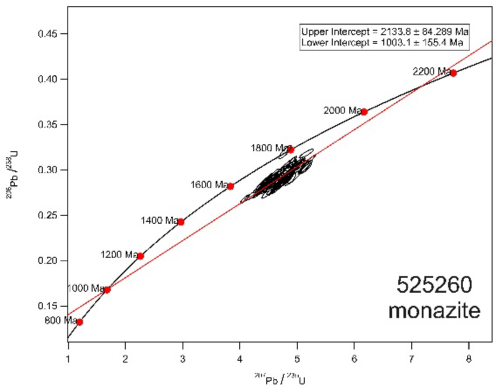
Upper Intercept = 2133.8 ± 84.289 Ma
Lower Intercept = 1003.1 ± 155.4 Ma
525260
monazite

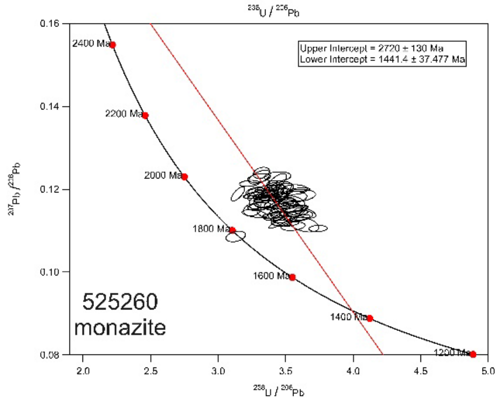
Upper Intercept = 2720 ± 130 Ma
Lower Intercept = 1441.4 ± 37.477 Ma
525260
monazite

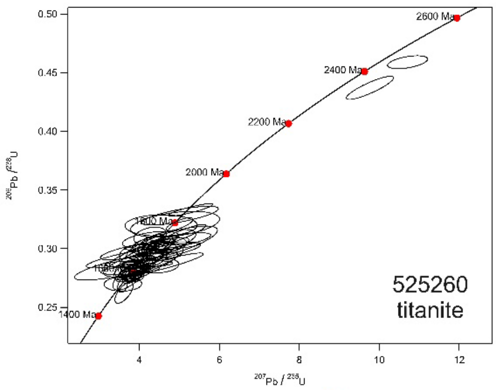
525260
titanite

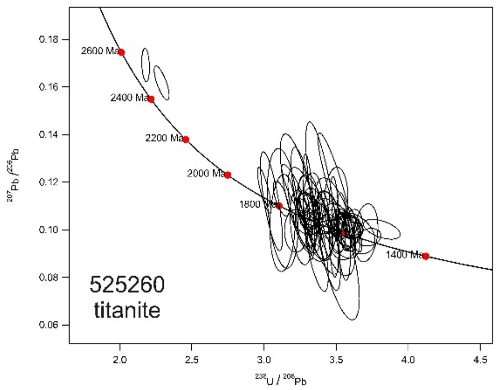
525260
titanite

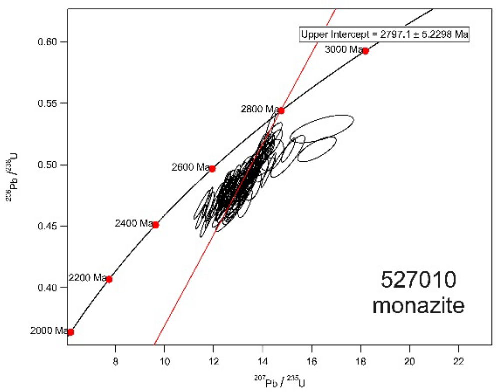
Upper Intercept = 2797.1 ± 5.2298 Ma
527010
monazite

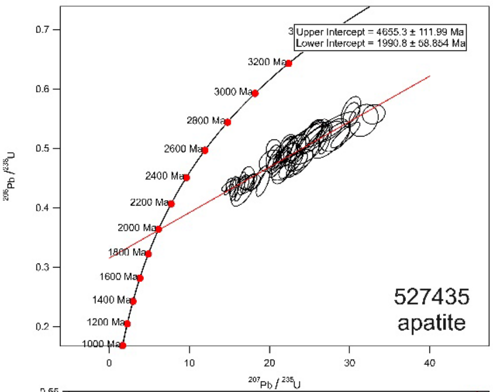
Upper Intercept = 4655.3 ± 111.99 Ma
Lower Intercept = 1990.8 ± 58.854 Ma
527435
apatite

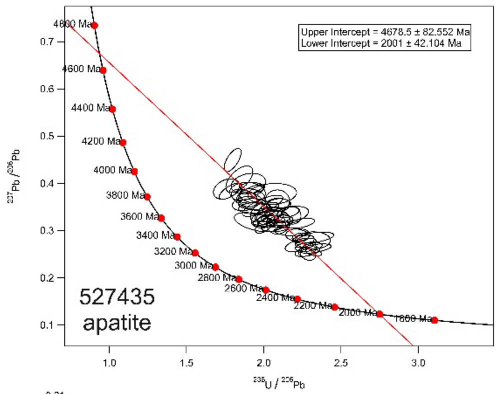
Upper Intercept = 4678.5 ± 82.552 Ma
Lower Intercept = 2001 ± 42.104 Ma
527435
apatite

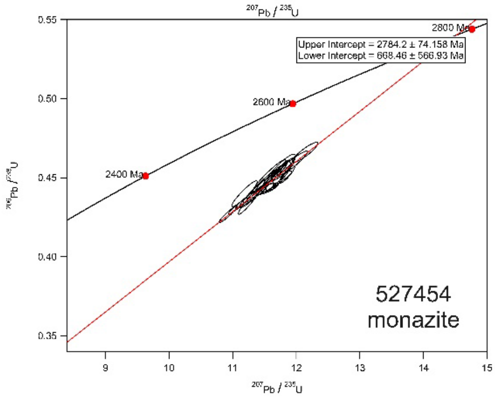
Upper Intercept = 2784.2 ± 74.158 Ma
Lower Intercept = 668.46 ± 566.93 Ma
527454
monazite

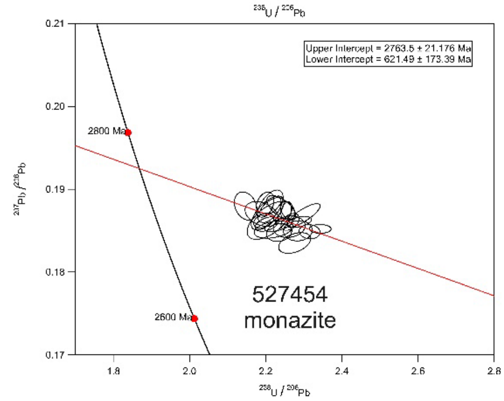
Upper Intercept = 2763.5 ± 21.176 Ma
Lower Intercept = 621.49 ± 173.39 Ma
527454
monazite

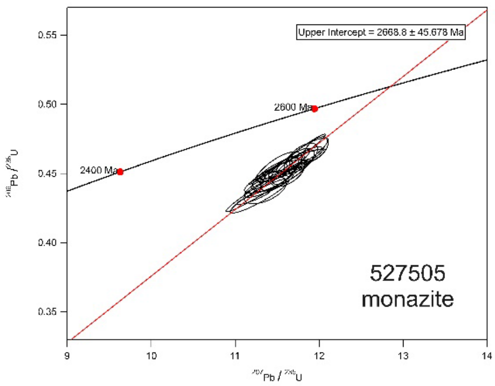
Upper Intercept = 2668.8 ± 45.678 Ma
527505
monazite

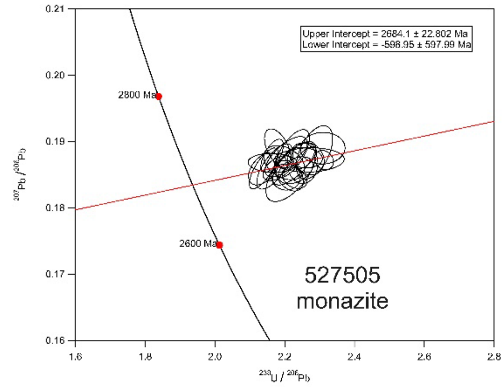
Upper Intercept = 2684.1 ± 22.802 Ma
Lower Intercept = -598.95 ± 597.99 Ma
527505
monazite

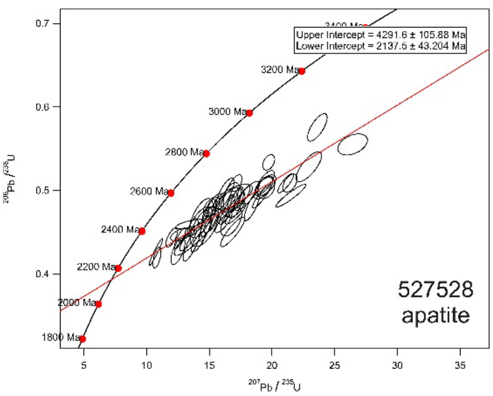
Upper Intercept = 4291.6 ± 105.88 Ma
Lower Intercept = 2137.5 ± 43.204 Ma
527528
apatite

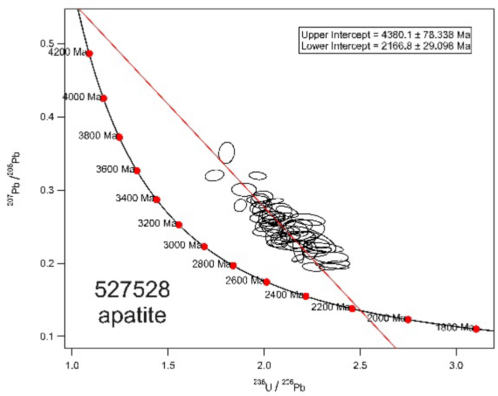
Upper Intercept = 4380.1 ± 78.338 Ma
Lower Intercept = 2166.8 ± 29.096 Ma
527528
apatite

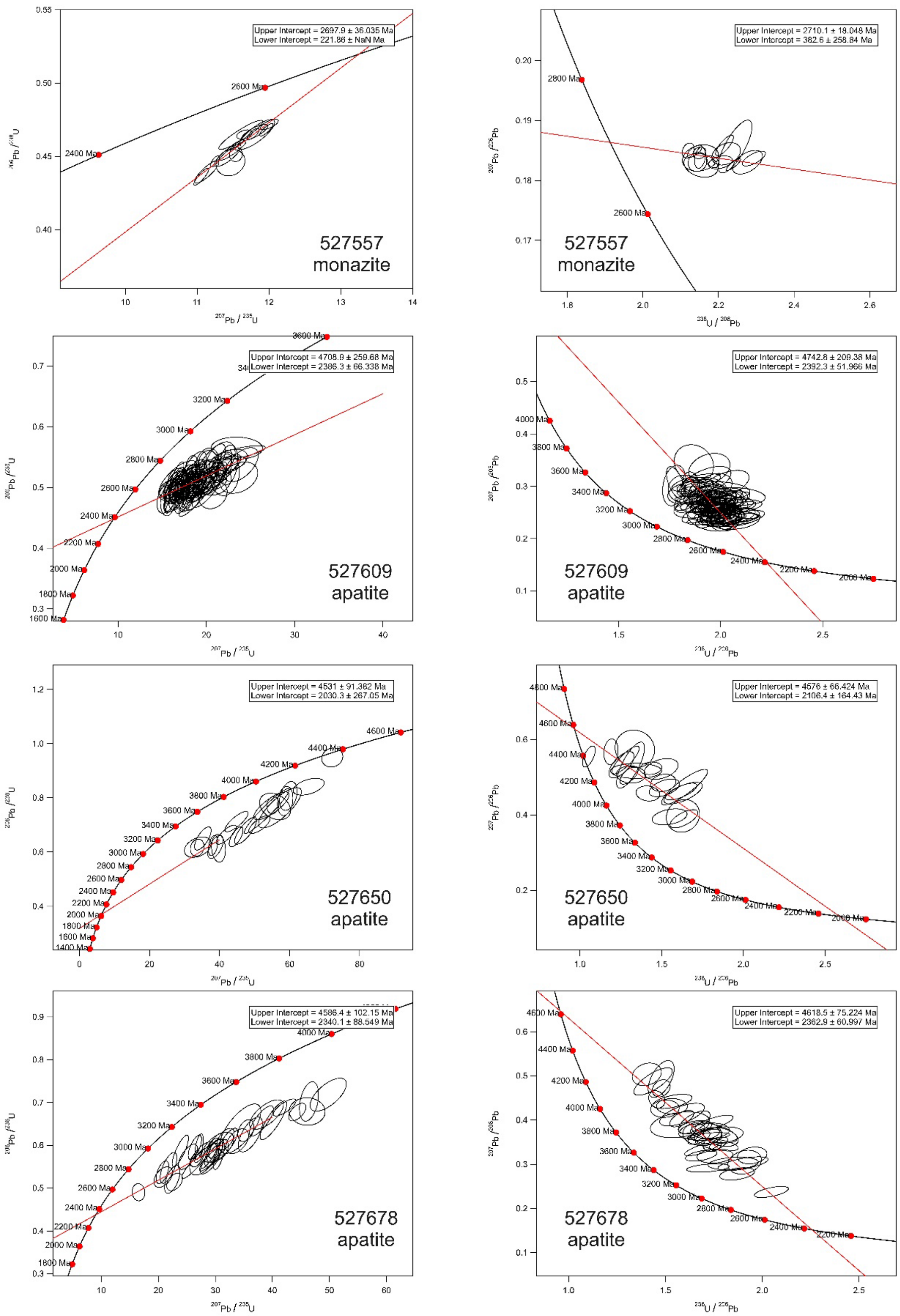
Upper Intercept = 2697.9 ± 36.035 Ma
Lower Intercept = 221.86 ± NaN Ma
527557
monazite
Upper Intercept = 2710.1 ± 18.048 Ma
Lower Intercept = 362.6 ± 258.84 Ma
527557
monazite
Upper Intercept = 4708.9 ± 259.68 Ma
Lower Intercept = 2386.3 ± 66.338 Ma
527609
apatite
Upper Intercept = 4742.8 ± 209.38 Ma
Lower Intercept = 2392.3 ± 51.966 Ma
527609
apatite
Upper Intercept = 4531 ± 91.382 Ma
Lower Intercept = 2030.3 ± 267.05 Ma
527650
apatite
Upper Intercept = 4576 ± 66.424 Ma
Lower Intercept = 2106.4 ± 164.43 Ma
527650
apatite
Upper Intercept = 4586.4 ± 102.15 Ma
Lower Intercept = 2340.1 ± 88.549 Ma
527678
apatite
Upper Intercept = 4618.5 ± 75.224 Ma
Lower Intercept = 2362.9 ± 60.997 Ma
527678
apatite

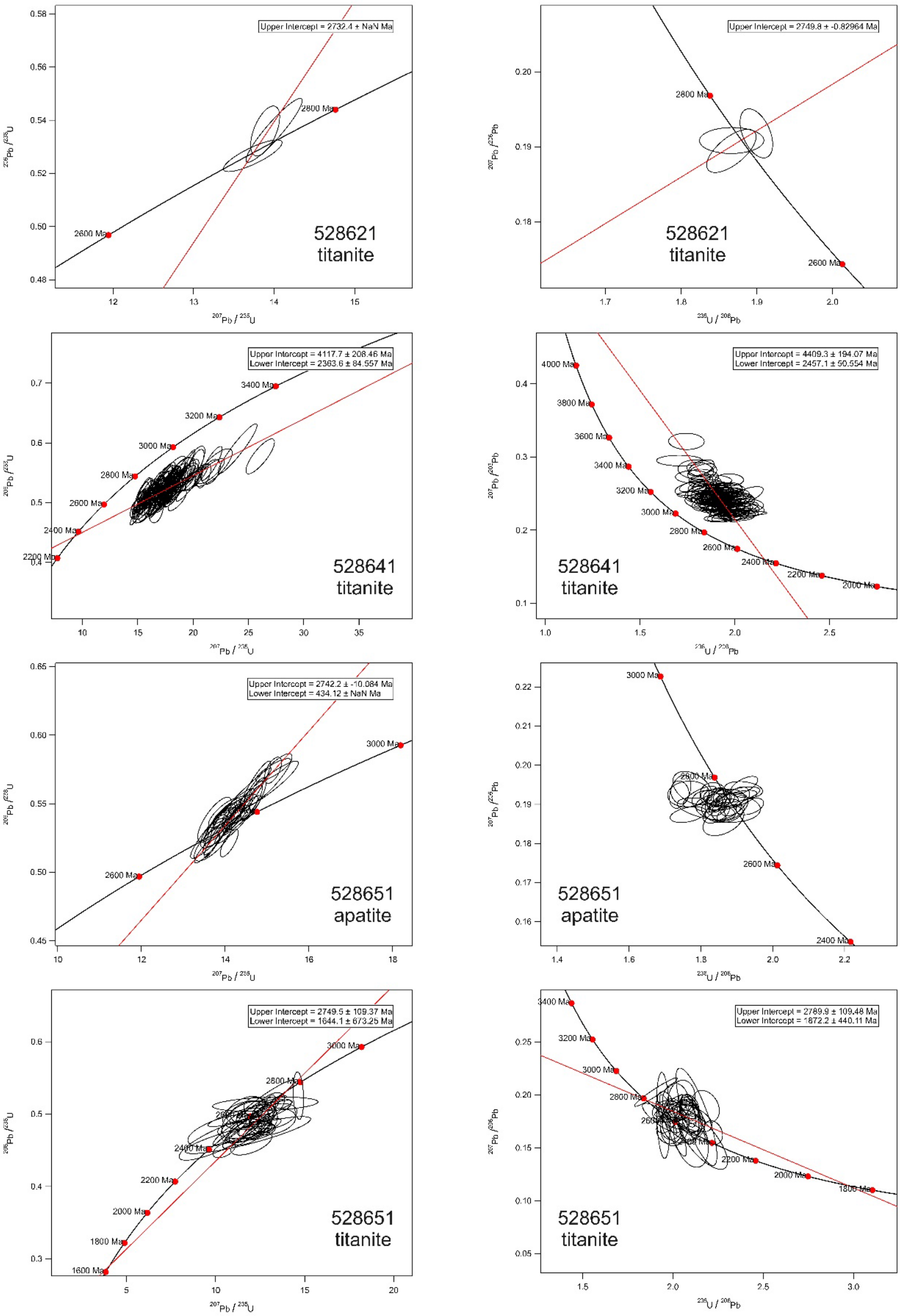
Upper Intercept = 2732.4 ± NaN Ma
528621
titanite
Upper Intercept = 2749.8 ± -0.82964 Ma
528621
titanite
Upper Intercept = 4117.7 ± 208.46 Ma
Lower Intercept = 2363.6 ± 84.557 Ma
528641
titanite
Upper Intercept = 4409.3 ± 194.07 Ma
Lower Intercept = 2457.1 ± 50.554 Ma
528641
titanite
Upper Intercept = 2742.2 ± -10.084 Ma
Lower Intercept = 434.12 ± NaN Ma
528651
apatite
528651
apatite
Upper Intercept = 2749.5 ± 109.37 Ma
Lower Intercept = 1644.1 ± 673.25 Ma
528651
titanite
Upper Intercept = 2789.9 ± 109.48 Ma
Lower Intercept = 1872.2 ± 440.11 Ma
528651
titanite

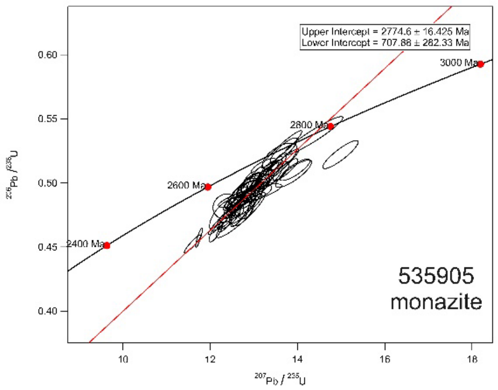
Upper Intercept = 2774.6 ± 16.425 Ma
Lower Intercept = 707.86 ± 282.33 Ma
535905
monazite

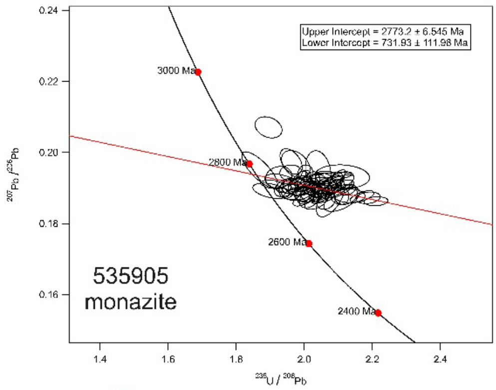
Upper Intercept = 2773.2 ± 6.545 Ma
Lower Intercept = 731.93 ± 111.98 Ma
535905
monazite

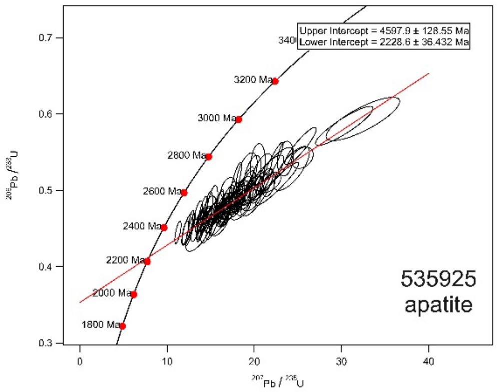
Upper Intercept = 4597.9 ± 128.55 Ma
Lower Intercept = 2228.6 ± 36.432 Ma
535925
apatite

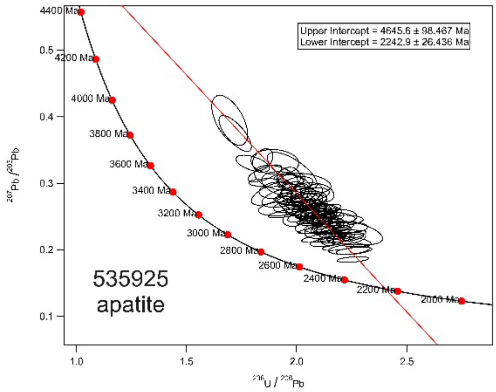
Upper Intercept = 4645.6 ± 98.467 Ma
Lower Intercept = 2242.9 ± 26.436 Ma
535925
apatite

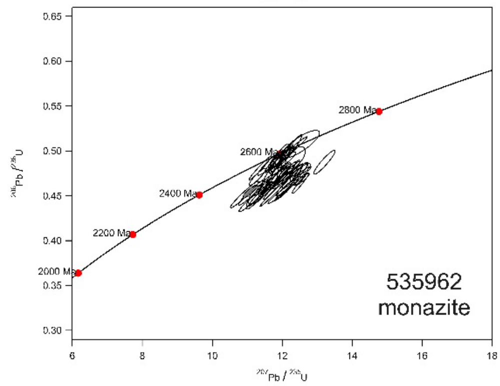
535962
monazite

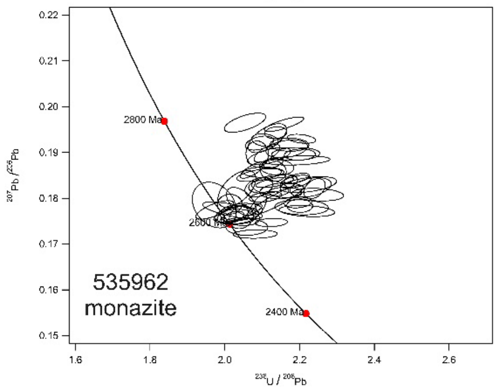
535962
monazite

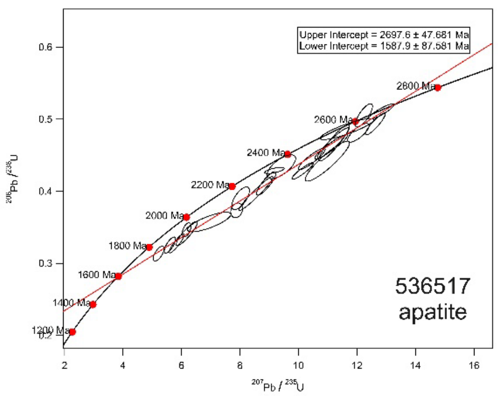
Upper Intercept = 2697.6 ± 47.681 Ma
Lower Intercept = 1587.9 ± 87.581 Ma
536517
apatite

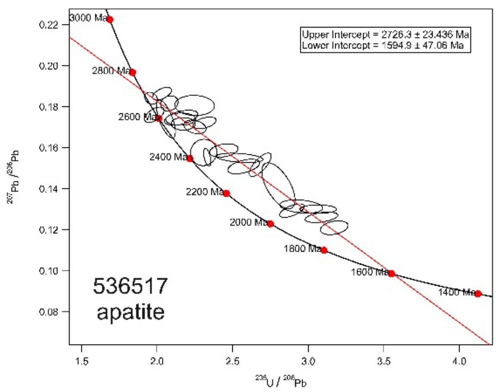
Upper Intercept = 2726.3 ± 23.436 Ma
Lower Intercept = 1594.9 ± 47.06 Ma
536517
apatite

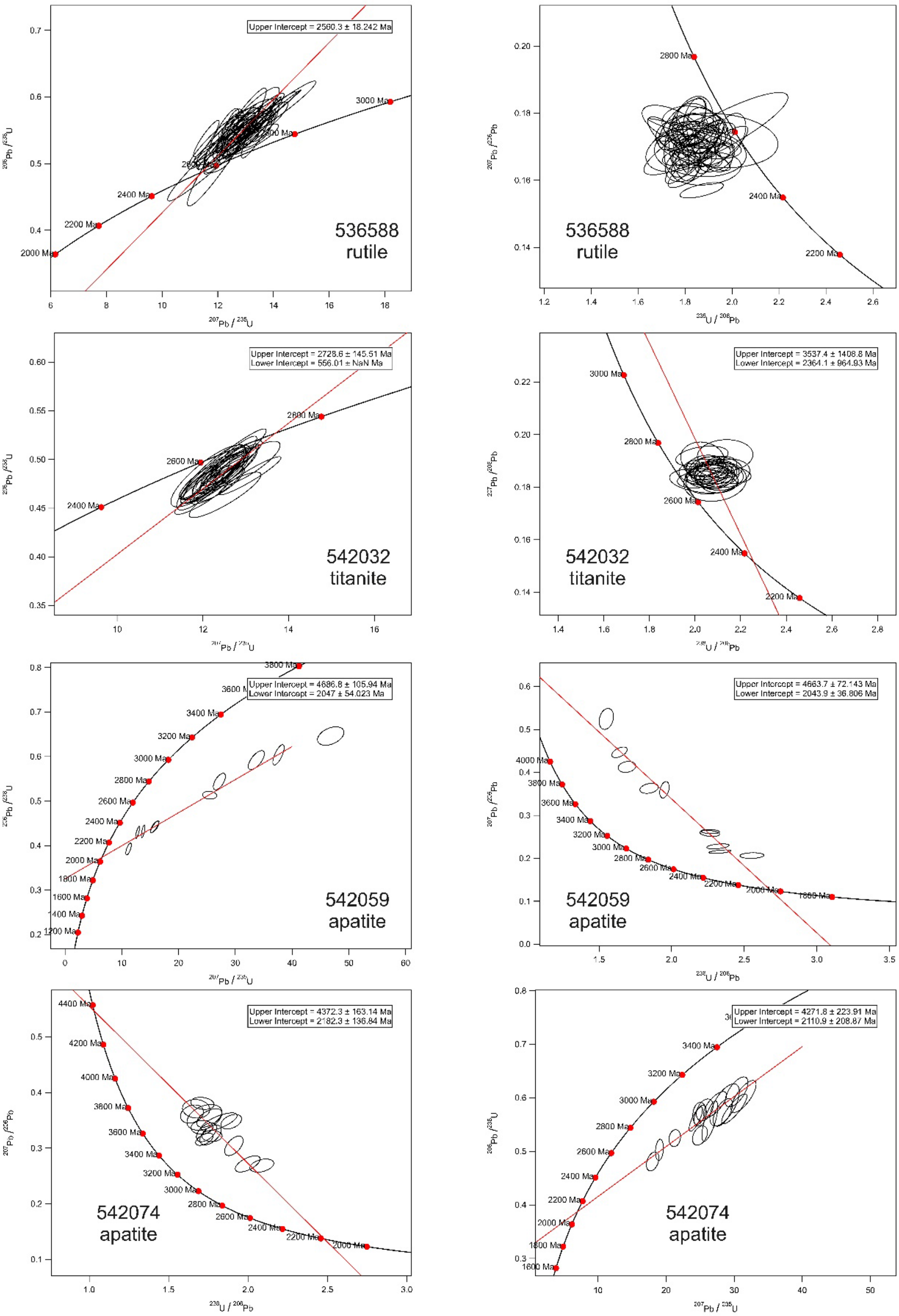
Upper Intercept = 2560.3 ± 18.242 Ma
536588
rutile
536588
rutile
Upper Intercept = 2728.6 ± 145.51 Ma
Lower Intercept = 556.01 ± NaN Ma
542032
titanite
Upper Intercept = 3537.4 ± 1408.8 Ma
Lower Intercept = 2364.1 ± 964.93 Ma
542032
titanite
Upper Intercept = 4686.8 ± 105.94 Ma
Lower Intercept = 2047 ± 54.023 Ma
542059
apatite
Upper Intercept = 4663.7 ± 72.143 Ma
Lower Intercept = 2043.9 ± 36.806 Ma
542059
apatite
Upper Intercept = 4372.3 ± 163.14 Ma
Lower Intercept = 2182.3 ± 136.84 Ma
542074
apatite
Upper Intercept = 4271.8 ± 223.91 Ma
Lower Intercept = 2110.9 ± 208.87 Ma
542074
apatite

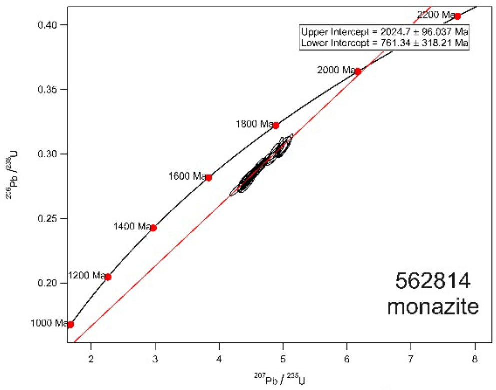
Upper Intercept = 2024.7 ± 96.037 Ma
Lower Intercept = 761.34 ± 318.21 Ma
562814
monazite
$^{207}Pb / ^{235}U$
$^{206}Pb / ^{238}U$

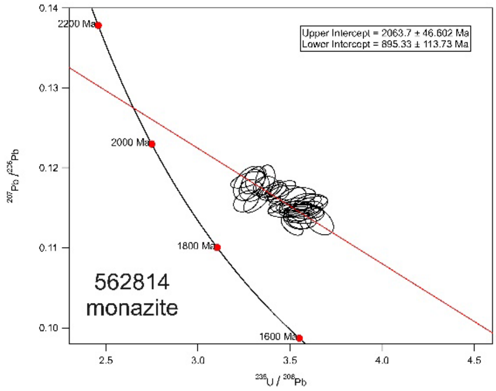
Upper Intercept = 2063.7 ± 46.602 Ma
Lower Intercept = 895.33 ± 113.73 Ma
562814
monazite
$^{238}U / ^{206}Pb$
$^{207}Pb / ^{206}Pb$

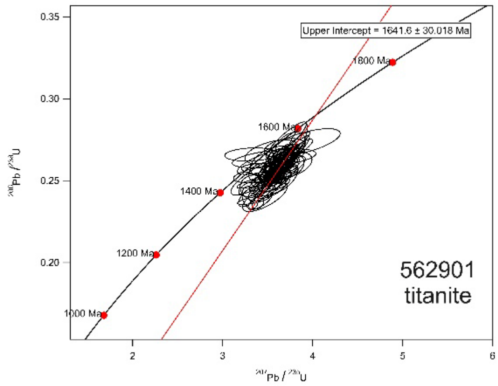
Upper Intercept = 1641.6 ± 30.018 Ma
562901
titanite
$^{207}Pb / ^{235}U$
$^{206}Pb / ^{238}U$

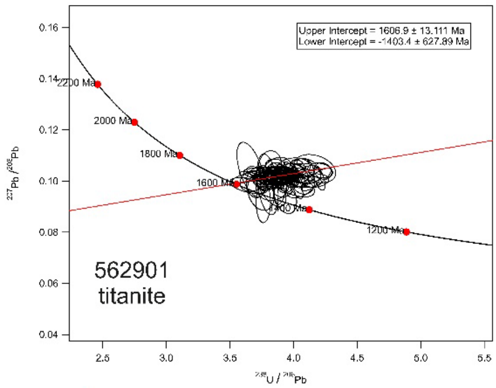
Upper Intercept = 1606.9 ± 13.111 Ma
Lower Intercept = -1403.4 ± 627.89 Ma
562901
titanite
$^{238}U / ^{206}Pb$
$^{207}Pb / ^{206}Pb$

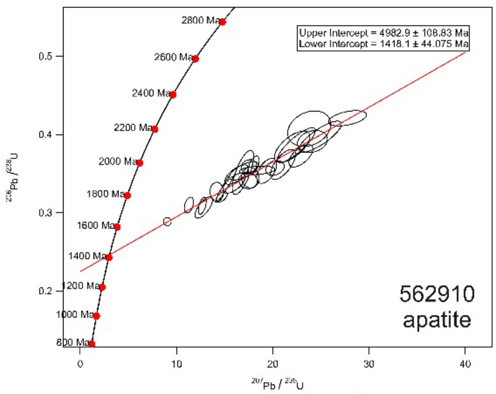
Upper Intercept = 4982.9 ± 108.83 Ma
Lower Intercept = 1418.1 ± 44.075 Ma
562910
apatite
$^{207}Pb / ^{235}U$
$^{206}Pb / ^{238}U$

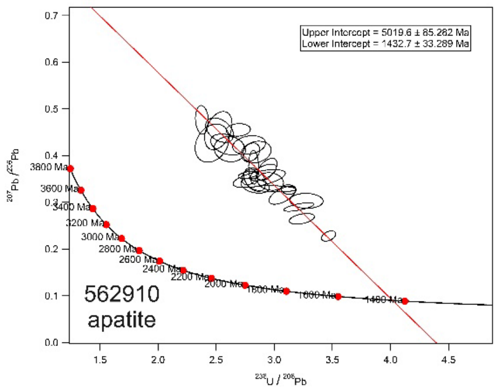
Upper Intercept = 5019.6 ± 85.282 Ma
Lower Intercept = 1432.7 ± 33.289 Ma
562910
apatite
$^{238}U / ^{206}Pb$
$^{207}Pb / ^{206}Pb$

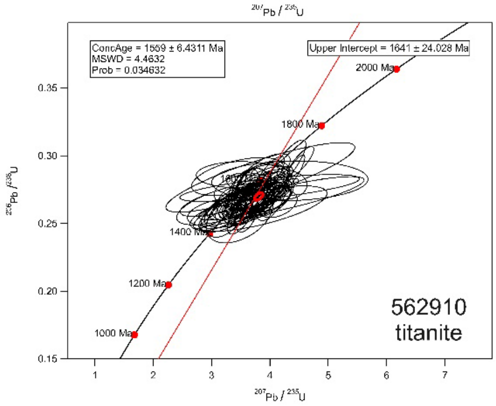
ConcAge = 1559 ± 6.4311 Ma
MSWD = 4.4632
Prob = 0.034632
Upper Intercept = 1641 ± 24.028 Ma
562910
titanite
$^{207}Pb / ^{235}U$
$^{206}Pb / ^{238}U$

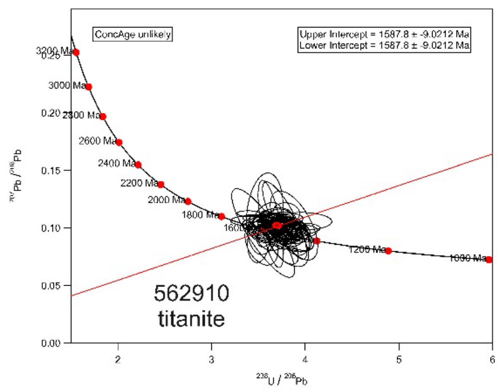
ConcAge unlikely
Upper Intercept = 1587.8 ± -9.0212 Ma
Lower Intercept = 1587.8 ± -9.0212 Ma
562910
titanite
$^{238}U / ^{206}Pb$
$^{207}Pb / ^{206}Pb$

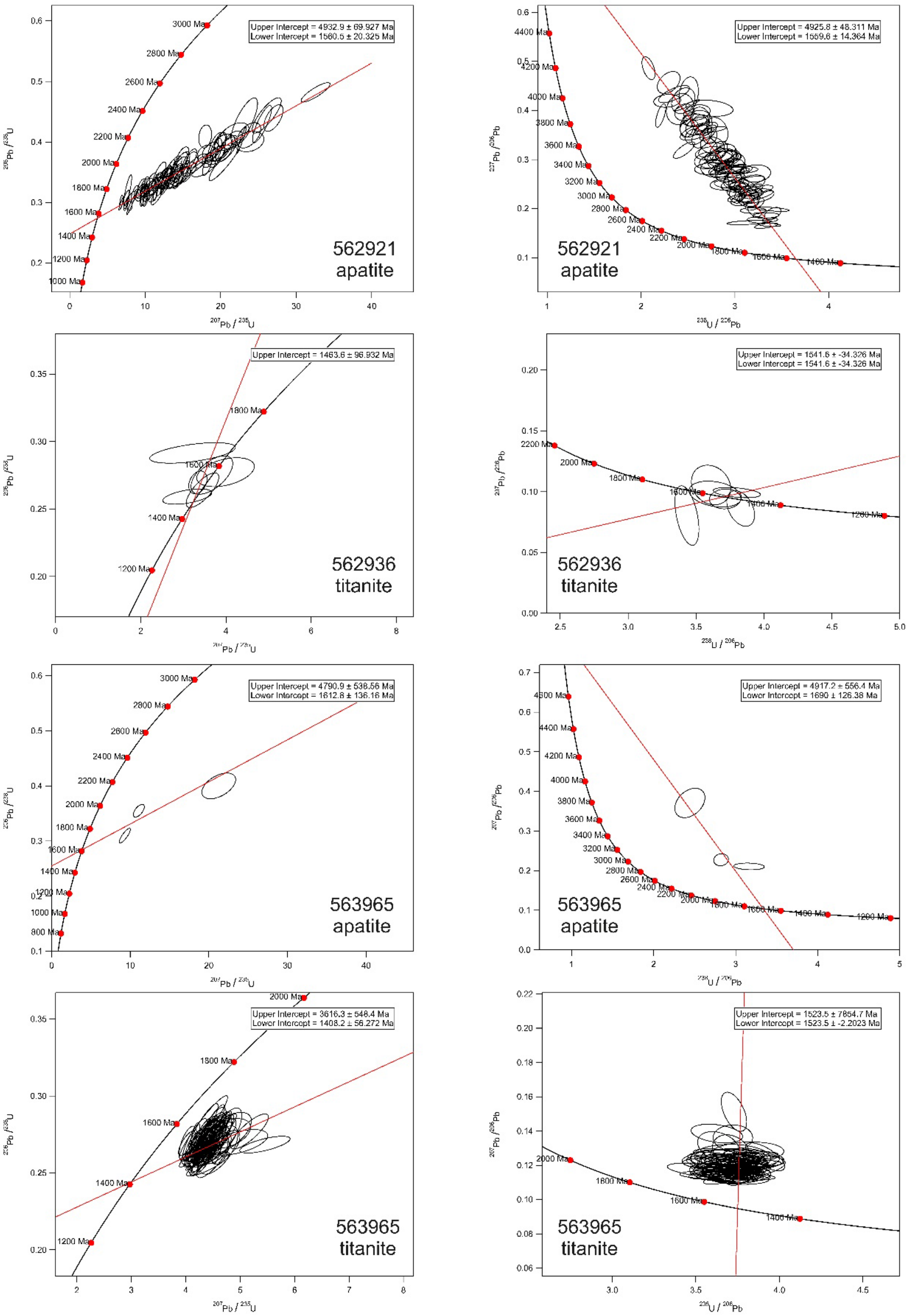
Upper Intercept = 4932.9 ± 69.927 Ma
Lower Intercept = 1560.5 ± 20.325 Ma
562921
apatite
Upper Intercept = 4925.8 ± 48.311 Ma
Lower Intercept = 1559.6 ± 14.364 Ma
562921
apatite
Upper Intercept = 1463.6 ± 96.932 Ma
562936
titanite
Upper Intercept = 1541.6 ± -34.326 Ma
Lower Intercept = 1541.6 ± -34.326 Ma
562936
titanite
Upper Intercept = 4790.9 ± 538.56 Ma
Lower Intercept = 1612.8 ± 136.16 Ma
563965
apatite
Upper Intercept = 4917.2 ± 556.4 Ma
Lower Intercept = 1690 ± 126.38 Ma
563965
apatite
Upper Intercept = 3616.3 ± 548.4 Ma
Lower Intercept = 1408.2 ± 56.272 Ma
563965
titanite
Upper Intercept = 1523.5 ± 7864.7 Ma
Lower Intercept = 1523.5 ± -2.2023 Ma
563965
titanite

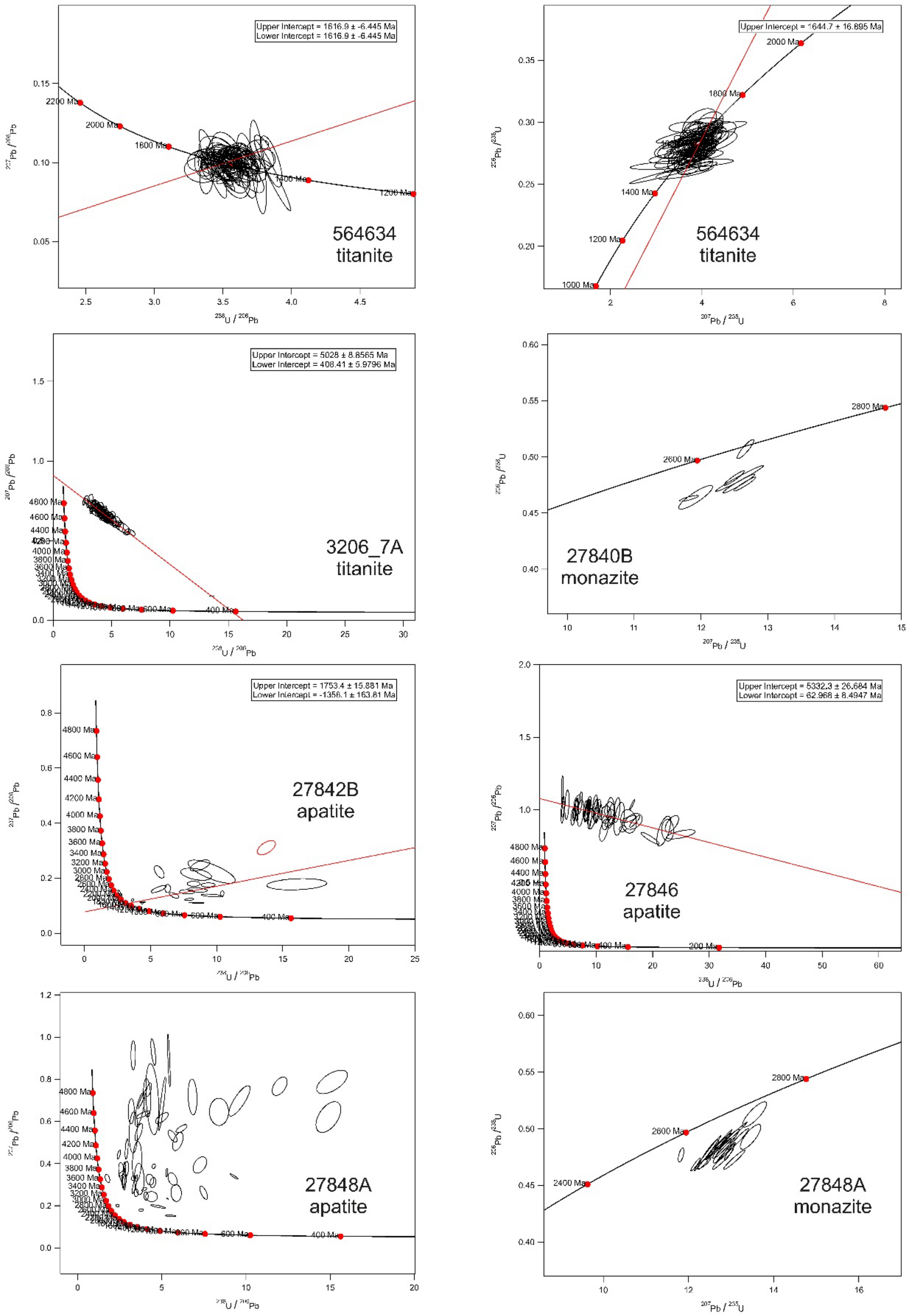

Upper Intercept = 1616.9 ± -6.445 Ma
Lower Intercept = 1616.9 ± -6.445 Ma
564634
titanite
Upper Intercept = 1644.7 ± 16.895 Ma
564634
titanite
Upper Intercept = 5028 ± 8.8565 Ma
Lower Intercept = 408.41 ± 5.9796 Ma
3206_7A
titanite
27840B
monazite
Upper Intercept = 1753.4 ± 15.881 Ma
Lower Intercept = -1356.1 ± 163.81 Ma
27842B
apatite
Upper Intercept = 5332.3 ± 26.684 Ma
Lower Intercept = 62.968 ± 8.4947 Ma
27846
apatite
27848A
apatite
27848A
monazite

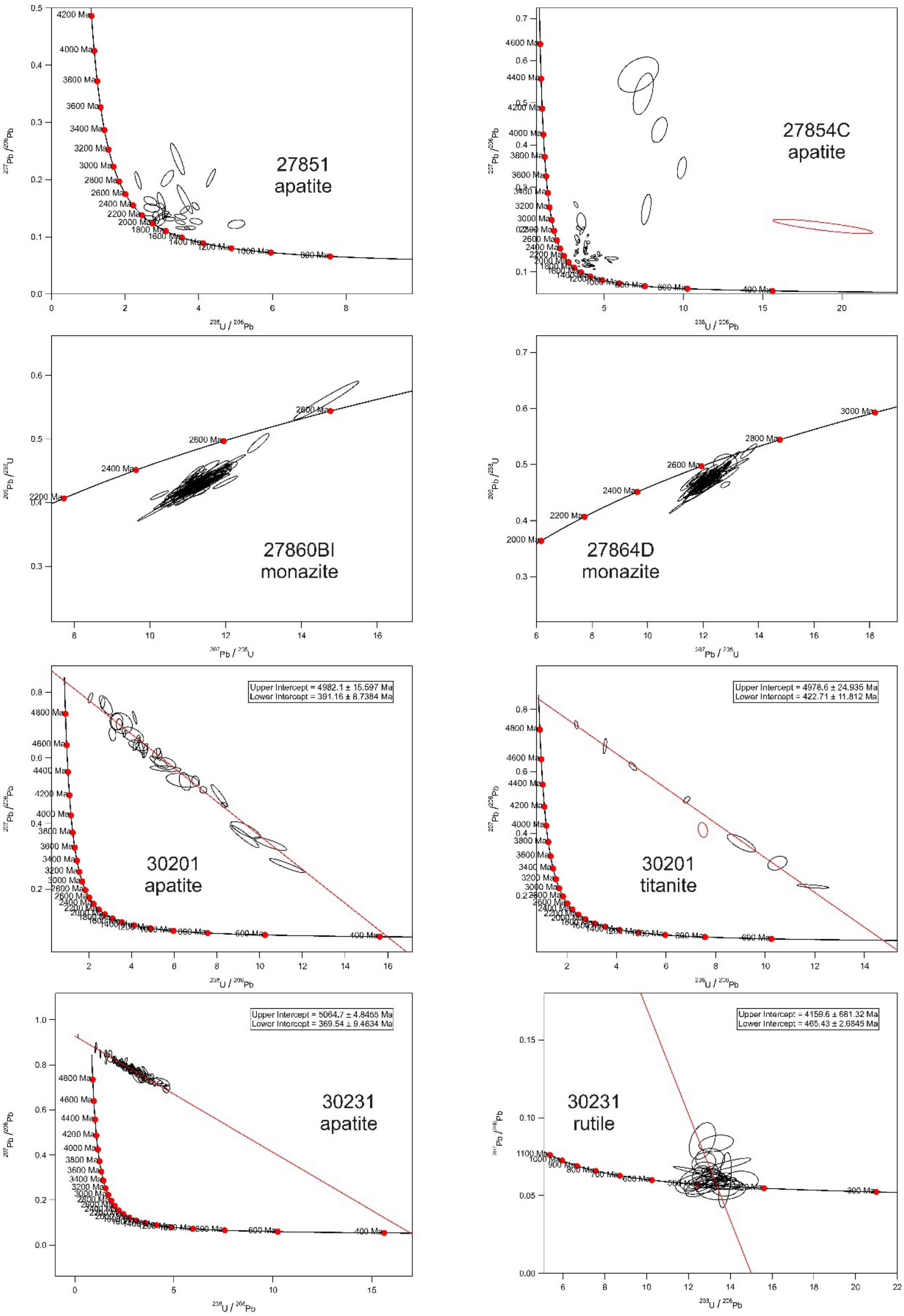
27851
apatite
27854C
apatite
27860BI
monazite
27864D
monazite
Upper Intercept = 4982.1 ± 15.597 Ma
Lower Intercept = 391.16 ± 8.7384 Ma
30201
apatite
Upper Intercept = 4978.6 ± 24.935 Ma
Lower Intercept = 422.71 ± 11.812 Ma
30201
titanite
Upper Intercept = 5064.7 ± 4.8455 Ma
Lower Intercept = 369.54 ± 9.4634 Ma
30231
apatite
Upper Intercept = 4159.6 ± 681.32 Ma
Lower Intercept = 465.43 ± 2.6845 Ma
30231
rutile

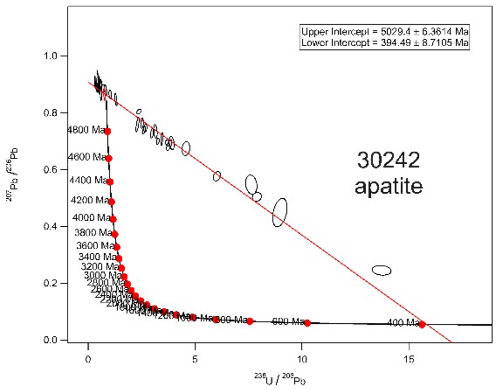
Upper Intercept = 5029.4 ± 6.3614 Ma
Lower Intercept = 394.49 ± 8.7105 Ma
30242
apatite

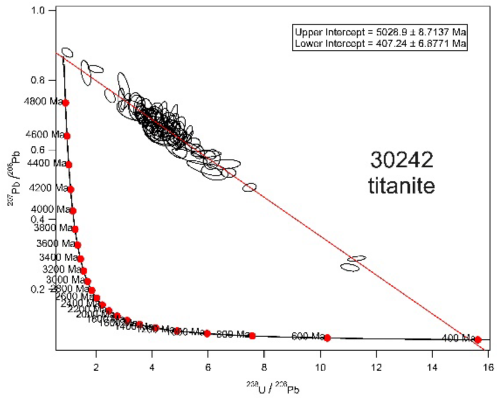
Upper Intercept = 5028.9 ± 8.7137 Ma
Lower Intercept = 407.24 ± 6.8771 Ma
30242
titanite

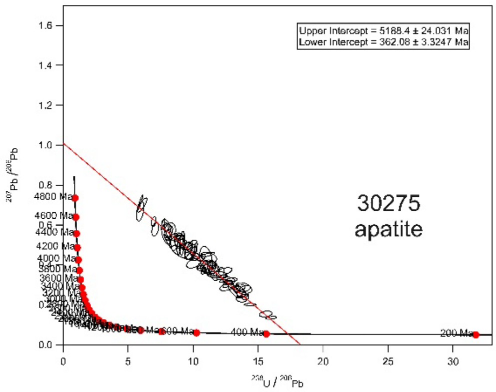
Upper Intercept = 5188.4 ± 24.031 Ma
Lower Intercept = 362.08 ± 3.3247 Ma
30275
apatite